

ALMA MATER STUDIORUM – UNIVERSITÁ DI BOLOGNA

DOTTORATO DI RICERCA IN SCIENZE BIOCHIMICHE E BIOTECNOLOGICHE

CICLO XXVIII

Settore concorsuale: 05 / E1

Settore scientifico – Disciplina: BIO12

Study of Magnesium homeostasis and intracellular  
compartmentalization in human cells by fluorescent chemosensors and  
Synchrotron X-ray fluorescence

Presentata da: Azzurra Sargenti

Coordinatore dottorato  
Prof. Santi Mario Spampinato

Relatore:  
Prof. Stefano Iotti

*Esame finale anno 2016*



# Table of Contents

<b>1</b>	<b>MAGNESIUM</b>	<b>6</b>
1.1	INTRODUCTION	6
1.2	Mg <sup>2+</sup> TRANSPORT ACROSS BIOLOGICAL MEMBRANE	6
1.2.1	Mg <sup>2+</sup> ACCUMULATION	8
1.2.1.1	TRPM Channels	9
1.2.1.2	MagT1	10
1.2.1.3	Claudins	10
1.2.1.4	CNNM Family	11
1.2.1.5	MRS2	11
1.2.1.6	MMgTs	12
1.2.2	Mg <sup>2+</sup> EXTRUSION	12
1.2.2.1	SLC41 Family	12
1.3	HORMONAL REGULATION OF Mg <sup>2+</sup> TRANSPORT AND HOMEOSTASIS	13
1.3.1	Mg <sup>2+</sup> EXTRUSION	14
1.3.2	Mg <sup>2+</sup> ACCUMULATION	14
1.4	MAGNESIUM AND CELL PROLIFERATION	15
1.5	MAGNESIUM AND CELL DIFFERENTIATION	17
<b>2</b>	<b>TECHNIQUES TO MEASURE MAGNESIUM</b>	<b>19</b>
2.1	INTRODUCTION	19
2.2	PRINCIPLE TECHNIQUES TO DETERMINE MAGNESIUM	19
2.3	FLUORESCENT CHEMOSENSORS	21
2.4	LAST GENERATION FLUORESCENT PROBES	22
2.4.1	THE KMG SERIES	22
2.4.2	KCM-1	23
2.4.3	AMG1 E AMG1-AM	24
2.4.4	THE DCHQS SERIES	24
2.4.5	MAGFRET	27
2.5	X-RAY MICROSCOPY	28
<b>3</b>	<b>AIMS</b>	<b>30</b>

<b>4</b>	<b>MATERIALS AND METHODS</b>	<b>33</b>
4.1	REAGENTS	33
4.2	CELL CULTURE	33
4.2.1	ADIPOSE- DERIVED STEM CELL ISOLATION	33
4.2.2	ADIPOSE- DERIVED STEM CELL TREATMENT	34
4.3	PHOTOPHYSICAL MEASUREMENTS	34
4.4	TITRATION OF $Mg^{2+}$ BINDING BY FLUORESCENCE SPECTROSCOPY	35
4.5	STABILITY OF THE PROBES	35
4.6	QUANTIFICATION OF TOTAL CELL MAGNESIUM BY AAS	35
4.7	QUANTIFICATION OF TOTAL CELL MAGNESIUM BY A SPECTROFLUORIMETRIC ASSAY	35
4.8	LIMIT OF DETECTION	36
4.9	FLOW CYTOMETRY	37
4.10	CELL CYCLE ANALYSIS	37
4.11	GENE EXPRESSION IN HASCs	37
4.12	FLUORESCENCE LIFETIME IMAGING (FLIM)	38
4.13	CELL CULTURE AND REAGENTS	41
4.14	QUANTIFICATION OF TOTAL CELL MAGNESIUM BY DCHQ5	42
4.15	DETERMINATION OF THE CELL VOLUME	42
4.16	FLUORESCENCE AND SCANNING TRANSMISSION X-RAY MICROSCOPY ANALYSIS	42
<b>5</b>	<b>RESULTS AND DISCUSSION</b>	<b>45</b>
5.1	STUDY OF THE ANALYTICAL CAPABILITIES OF DCHQ5 FOR THE QUANTITATIVE ASSESSMENT OF TOTAL INTRACELLULAR $Mg$ CONTENT	45
5.1.1	PHOTOPHYSICAL PROPERTIES OF DCHQ5	45
5.1.2	DESIGN OF A NEW PROTOCOL FOR THE QUANTITATIVE ASSESSMENT OF TOTAL INTRACELLULAR MAGNESIUM	47
5.1.3	CYTOFLUORIMETRIC ASSAYS IN VIABLE CELLS	50
5.2	FLUORESCENCE LIFETIME IMAGING OF DCHQ5	52
5.3	STUDY OF THE MAGNESIUM INVOLVEMENT IN THE COMMITMENT OF HUMAN ADIPOSE-DERIVED MESENCHYMAL STEM CELLS	55
5.3.1	TOTAL MAGNESIUM CONTENT AND CELL CYCLE ANALYSES OF HASCs IN COMPLETE AND $Mg$ -FREE MEDIUM	55

5.3.2 ANALYSES OF GENE EXPRESSION OF A PANEL OF MULTILINEAGE MARKERS IN COMPLETE AND MG-FREE MEDIUM	59
<b>6 CONCLUSIONS</b>	<b>76</b>
<b>REFERENCES</b>	<b>78</b>

# 1 MAGNESIUM

## 1.1 Introduction

Magnesium ( $Mg^{2+}$ ) is an essential ion to the human body, being the most abundant divalent intracellular cation in the cells, the second most abundant cellular ion next to potassium, and the fourth cation in general in the human body [1].

Total body magnesium (Mg) content in the average 70 kg adult is approximately 25 g [2], of which 50-60% resides in bone, while the remaining 40 % are located extra- and intracellular [3].

Inside the cell magnesium is responsible for a plethora of functions, from the activation of a variety of enzymes to the signal-transduction proteins. It is also required for trans-cellular ion transport, membrane stabilization, cytoskeletal activity, synthesis of carbohydrates, proteins, lipids and nucleic acids [3], [4]. Furthermore, cellular energy metabolism is strictly dependent on magnesium availability, since the functional ATP form is  $MgATP^{2-}$  [5], [6].

As a consequence, being implicated in those reactions utilizing ATP or catalyzing the transfer of phosphate,  $Mg^{2+}$  plays a role in virtually every process in the cell [4]. On the base of these findings, is not surprising that reduction of magnesium availability is implicated in many human disease, such as hypertension, heart defects, nervous system disorder, muscle disease, atherosclerosis, diabetes and metabolic syndrome [3], [7], [8].

## 1.2 $Mg^{2+}$ transport across biological membrane

Total intracellular magnesium concentration ranging between 17 and 20 mM in mammalian cells [9]. The cellular distribution of magnesium is heterogeneous, with lower concentrations in the peripheral regions of the cytoplasm than in the perinuclear region [10]. The majority of cellular  $Mg^{2+}$  is bound to proteins,

phospholipids, nucleic acids and especially ATP [9], or it is sequestered within mitochondria and endoplasmic reticulum, which are the main intracellular  $Mg^{2+}$  stores. The majority of cytoplasmic  $Mg^{2+}$  is present in the form bound to ATP and phosphometabolites, so cytosol free ionized  $Mg^{2+}$  represents only a small amount, approximately 5% of the total cellular Mg. The free  $Mg^{2+}$  concentration is  $\approx 0.2\text{--}1$  mM [11], [12], and it is maintained below the concentration predicted from the transmembrane electrochemical potential. This control is achieved through a balance of  $Mg^{2+}$  uptake, intracellular  $Mg^{2+}$  storage and  $Mg^{2+}$  efflux.

Taking into account that the membrane potential typically ranges from  $-40$  mV to  $-80$  mV (negative on the cytoplasmic side) and that the extracellular concentration of magnesium is higher than its intracellular ones [13]–[15], uptake of  $Mg^{2+}$  into the cell can be mediated by channels or channel-like mechanisms.

On the contrary, outward transport of cations takes place against the electrochemical gradient, therefore,  $Mg^{2+}$  extrusion must be accomplished by an ATP-dependent transporter or by an exchanger.

Of great interest for the feature of  $Mg^{2+}$  transporters are the peculiar chemical properties of  $Mg^{2+}$ , properties that make it unique amongst biological cations. Indeed, in the dissolved state,  $Mg^{2+}$  has two hydration shells, making its hydrated radius 400-times larger than its dehydrated radius, larger than that of other cations like  $Na^+$ ,  $K^+$ , and even  $Ca^{2+}$  [16]. For instance, it is almost impossible for magnesium to pass through narrow channels in biological membranes because magnesium cannot be easily stripped of its hydration shell [2]. Steric constraints for magnesium transporters are also far greater than for any other cation transport system [16]: proteins transporting magnesium are required to recognize the large hydrated cation, strip off its hydration shell and deliver the bare ion to the transmembrane transport pathway through the membrane, a process that requires a lot of energy [8].

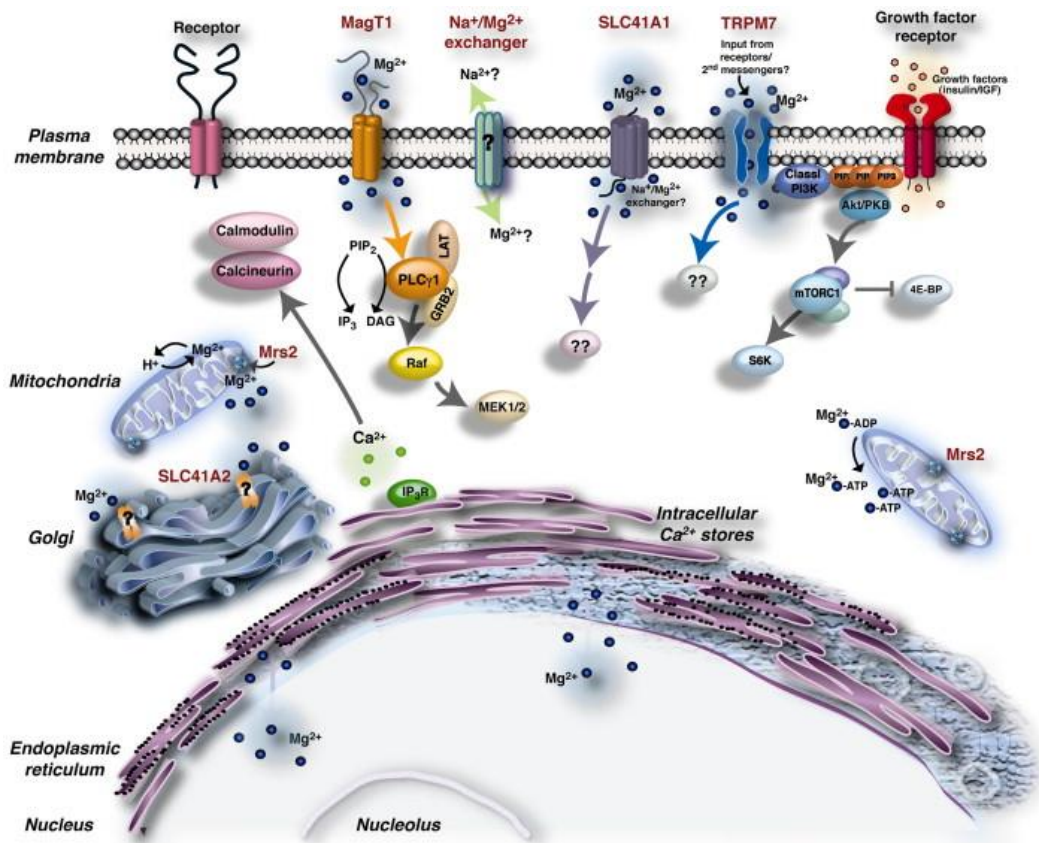


**Figure 1.1: Mg<sup>2+</sup> transport in vertebrate cells** [17]. The figure depicted various proposed Mg<sup>2+</sup> transporters and their predicted transport mechanisms: **Mrs2**, a mitochondrial Mg<sup>2+</sup> uptake system that transports Mg<sup>2+</sup> with mitochondrial membrane potential (channel transport mechanism based on similarity with yeast Alr family); TRPM7 channel kinase (channel transport mechanism), and MagT1 (thought to be a plasma membrane Mg<sup>2+</sup> transporter with an ion channel transport mechanism). SLC41A1/A2 (channel transport mechanism based on structural homology with prokaryotic MgtE transporters): SLC41A1 identified as the Na<sup>+</sup>/Mg<sup>2+</sup> exchanger [18] represents an exchange mechanism which mediates Mg<sup>2+</sup> efflux in vertebrate cells; SLC41A2 has been suggested as the responsible Mg<sup>2+</sup> transporter in Golgi but its mode of operation is still uncovered. Mg<sup>2+</sup> transport into both the endoplasmic reticulum and nucleus are very poorly characterized and hence are pictured simply as passive exchange mechanisms (Taken from Sahni et al, 2013).

### 1.2.1 Mg<sup>2+</sup> accumulation

The majority of the recently identified Mg<sup>2+</sup> entry mechanisms operate at the cell membrane level with two notable exceptions that favor Mg<sup>2+</sup> transport across the membrane of mitochondria and Golgi system, respectively [15].

### 1.2.1.1 TRPM Channels

Transient receptor potential (TRP) cation channels represent a large family of ion channels that are expressed in several organisms, tissues and cell types and act as important transducers in cellular communication network. The TRP superfamily is divided into six related sub family proteins, including the TRPM sub family members [19].

The melastatin-related TRP family (TRPM) consists of eight members that can be group into four pairs based on amino acid sequence similarities: TRPM1/3, TRPM2/8, TRPM4/TRPM5 and TRPM6/7.

TRPM7 and TRPM6 were the first  $Mg^{2+}$  channels identified in mammalian cells and they both shared the unique feature of a kinase domain belonging to the atypical family of alpha-kinases at their C-terminus fused to the ion channel domain for which they have been termed '*chanzymes*' (*channels plus enzymes*) [20]. TRPM6 and TRPM7 are able to build heteromultimers [21], and share many biophysical and biochemical properties, but their kinase do not have identical substrate specificities. In particular, TRPM6 and TRPM7 both autophosphorylate threonine residues, but only TRPM6 crossphosphorylate TRPM7, and not the reverse [22].

While TRPM7 is equally distributed in human tissues and organs, the expression of TRPM6 is localized in the colon and in the distal convoluted tubule of the nephron, where it represents the key protein in the transcellular pathway of intestinal  $Mg^{2+}$  absorption and renal reabsorption [23], although recent studies indicate that TRPM6 might have a broader expression pattern, specifically in cells of the immune system [24]. Moreover, impairment of TRPM6 expression has been associate to a genetic form of hypomagnesemia accompanied by hypocalcemia poorly restored by massive  $Mg^{2+}$  administration [25], [26].

While TRPM7 shares a very high homology with TRPM6, genetical studies demonstrated that TRPM7 and TRPM6 fulfill non-redundant functions and that each channel contributes uniquely to the regulation of  $Mg^{2+}$  homeostasis [27]. Accordingly, they do not complement for each other's deficiency in TRPM7<sup>-/-</sup> B lymphocyte [28], in TRPM6<sup>-/-</sup> and TRPM7<sup>-/-</sup> mice [29], [30].

TRPM7 is important to ensure a rapid  $Mg^{2+}$  entry during G1 phase of the cell cycle and its activity is regulated by intracellular  $Mg^{2+}$  through a negative feedback mechanism [30]. It is considered a master regulator of cellular  $Mg^{2+}$  homeostasis and it is involved in a number of vital cellular processes in mammalian cells. Furthermore, recently TRPM7 has gaining increasing attention for its potential role in cancers as a new diagnostic and prognostic marker, in addition to known biomarkers [31].

#### **1.2.1.2 MagT1**

Currently, the only known selective plasma membrane  $Mg^{2+}$  transporter is MagT1. It has been demonstrated to be essential for vertebrate  $Mg^{2+}$  influx [32], and is broadly expressed in human tissues [33].

A recent study shows that in the situation of TRPM7-deficiency, eukaryotic DT40 B cells (chicken B-cell line) increase the expression level of MagT1, indicating that MagT1 might compensate for the lack of TRPM7 [34]. A further study [33], characterizes MagT1 and TUSC3, its human paralogue, as major mechanisms of  $Mg^{2+}$  influx, as a knockdown of either MagT1 or TUSC3 significantly lowers the total and free intracellular  $Mg^{2+}$  concentrations in mammalian cell lines. Moreover, it is reported that magnesium, and in particular MagT1 channel, are key molecular players for T cell activation and cytotoxic activity [35].

#### **1.2.1.3 Claudins**

Claudin-16 was the first  $Mg^{2+}$  transporting protein to be identified in mammals, and is a member of the claudin family, which comprehends a group of tight junction proteins.

Claudin-16 mediates paracellular  $Ca^{2+}$  and  $Mg^{2+}$  fluxes throughout the nephron, which is thought to be the main renal  $Mg^{2+}$  reabsorption mechanism.

Mutations in Claudin-16 are responsible for a hereditary disease called hypomagnesemia with hypercalciuria and nephrocalcinosis (FHHNC), characterized by massive renal  $Mg^{2+}$  and  $Ca^{2+}$  wasting [36].

Recently another claudin isoform, Claudin-19, has been shown to be involved in the reabsorption of  $Mg^{2+}$  and  $Ca^{2+}$  [37]. This protein forms a heteromeric complex with

Claudin-16 at the level of the tight junction, with specific cation-selectivity. Point mutations of both of these proteins affect the heteromeric interaction leading to development of FHHNC [5].

#### **1.2.1.4 CNNM Family**

The cyclin M (CNNM) family, also known as the ancient conserved domain protein (ACDP) family, consists of four proteins (CNNM1–4 or ACDP1–4) in mammals [38]. The name results from a weak sequence similarity that is shared with the cyclin family, although a cyclin-like function has never been shown for CNNM1–4 [39]. CNNMs reside at the plasma membrane where CNNM1 has been identified as a cytosolic copper chaperone, CNNM2 was shown to mediate  $Mg^{2+}$ -sensitive  $Na^+$  currents during the regulation of renal  $Mg^{2+}$  uptake, CNNM3 and CNNM4 have been linked with serum  $Mg^{2+}$  levels [40], [41].

Mutations in the CNNM2 gene cause familial dominant hypomagnesaemia, a rare human disorder characterized by renal and intestinal  $Mg^{2+}$  wasting [41], and CNNM2 has been also associated with coronary artery disease and hypertension [42].

Recently, it has been found that CNNM3 activity is regulated by the oncogene PRL2 and that his interaction could be essential for  $Mg^{2+}$  influx that drives tumour progression. Taking into account these results, CNNM3 seems to be involved in cancer [43].

#### **1.2.1.5 MRS2**

The only known transporter in eukaryotic cells responsible for  $Mg^{2+}$  uptake into mitochondria is MRS2.  $Mg^{2+}$  transport into the mitochondrial matrix occurs via electrophoretic uniport, driven by the mitochondrial membrane potential [44]. MRS2 protein is required for normal mitochondrial  $Mg^{2+}$  homeostasis and function, and also for the stability of mitochondrial respiratory complexes [45].

MRS2 expression has also been associated to drug resistance of gastric cancer cells where it was observed an up-regulation of this channel in doxorubicin resistant cells respect to the sensitive counterparts; vice versa, MRS2 knock down partially reverse the MDR phenotype in cells with acquired resistance [46].

Taking into account these findings, it seems that MRS2 overexpression might counteract drug-induced apoptosis by increasing magnesium influx into mitochondria [47].

#### **1.2.1.6 MMgTs**

The membrane  $Mg^{2+}$  transporter (MMgTs) gene family comprehends two proteins, MMgT1 and MMgT2, with no known similarities to other transporters. MMgT1 and MMgT2 are specifically located in the Golgi complex and post-Golgi vesicles, in which they contribute to regulate  $Mg^{2+}$ -dependent enzymes involved in protein assembly. MMgT1 and MMgT2 transcripts are present in a wide variety of tissues, suggesting a housekeeping role for the two transporters in cellular  $Mg^{2+}$  metabolism. Moreover, the small size of these proteins suggests that they form homo- and/or hetero-oligomeric channels to favor  $Mg^{2+}$  permeation [9], [36].

#### **1.2.2 $Mg^{2+}$ extrusion**

Two mechanisms were postulated to mediate  $Mg^{2+}$  extrusion. The first mechanism uses the  $Na^+$  concentration gradient as only energy input for the extrusion of  $Mg^{2+}$  and the mechanism was therefore named  $Na^+$ -dependent exchanger. To mediate  $Mg^{2+}$  extrusion,  $Na^+$ -dependent exchanger requires a physiological concentration of  $Na^+$  in the extracellular milieu, suggesting that the mechanism occurs through a  $Na^+/Mg^{2+}$  exchanger by the extrusion of 1 Mg in exchange with 2 Na [15]. Recently, this exchanger has been molecularly identified as being the solute carrier family 41 member A1 (SLC41A1) [18].

The second mechanism is  $Na^+$  independent and still remains poorly characterized. Different cations (e.g.  $Ca^{2+}$  or  $Mn^{2+}$ ) and anions (e.g.  $HCO_3^-$ ,  $Cl^-$ ) are suspected to act as counter-ions in this process [48].

##### **1.2.2.1 SLC41 Family**

The 41st family of solute carriers (SLC41) comprises three members, SLC41A1, SLC41A2 and SLC41A3, which have been found in all eukaryotes and are distantly homologous to bacterial  $Mg^{2+}$  channel MgtE [49]–[51].

SLC41A1 is the only member that has been well characterized at the molecular and physiological level, and as mentioned above, it has been recently identified as the  $\text{Na}^+/\text{Mg}^{2+}$  exchanger mediating  $\text{Mg}^{2+}$  transport across the plasma membrane [18]. Little is known about the exact function of SLC41A2 and SLC41A3, however, based on their homology with A1, it could be assumed, that both A2 and A3 also function as  $\text{Mg}^{2+}/(\text{X}^+)$  carriers, and in particular SLC41A2 seems to be primarily functional in the membranes of the intracellular compartments mediating  $\text{Mg}^{2+}$  subcellular transport [52].

SLC41A1 is ubiquitously expressed in human cells, while no information exists about the expression of human A2 and A3 across human tissues and organs.

Several reports have recently been published linking SLC41A1 (as a key component of cellular and perhaps also of systemic  $\text{Mg}^{2+}$  homeostasis) with serious human illnesses. Among the most exciting findings has been the discovery that A1 is part of a novel Parkinson's disease (PD) susceptibility locus PARK16, and it seems that single nucleotide-polymorphisms (SNPs) of SLC41A1 are linked to PD [53], [54].

Moreover, a link between preeclampsia and elevated expression of A1 in placental tissues has been recently demonstrated, suggesting that A1 carried out an important role in the pathophysiology of this disease [55].

### **1.3 Hormonal Regulation of $\text{Mg}^{2+}$ Transport and Homeostasis**

Under resting conditions, mammalian cells tightly regulate their basal  $\text{Mg}^{2+}$  content within the range of 17-20 mM even when a major trans-membrane gradient is artificially imposed [9].

At the same time, several papers demonstrated the occurrence of large  $\text{Mg}^{2+}$  fluxes, in either direction across the cell membrane and the membrane of intracellular stores following metabolic stimulations by hormonal and pharmacological factors including  $\beta$ -agonists, growth factors, and insulin [56]–[58].

### 1.3.1 Mg<sup>2+</sup> Extrusion

In the majority of eukaryotic cells, hormones or agents that increase intracellular cAMP level, such as catecholamines, glucagon, arachidonic acid or forskolin, provoke a significant extrusion of Mg<sup>2+</sup> into the extracellular space by the activity of Na<sup>+</sup>/Mg<sup>2+</sup> exchangers. Indeed, it has been shown that many different cellular types, from cardiac cells [59] to lymphocyte [60] among other cells [61], respond with a massive Mg<sup>2+</sup> efflux returning to baseline levels within 8 minutes from the application of the stimulus. This large and temporally limited Mg<sup>2+</sup> fluxes may lead to a significant redistribution and mobilization of Mg<sup>2+</sup> across the cells and cell compartments, which can affect many cellular functions and metabolic pathways. The key role of cAMP mediated extrusion is further corroborated by the observation that pre-treatment of cells with hormones or agents that decrease cAMP levels, are able to prevent cellular Mg<sup>2+</sup> mobilization [56], [60].

Furthermore, either the removal of extra cellular Na<sup>+</sup> or its replacement with non-selective Na<sup>+</sup>/Mg<sup>2+</sup> exchanger inhibitors like imipramine and quinidine, abolishes the Mg<sup>2+</sup> extrusion almost completely. These clearly indications that cAMP-mediated Mg<sup>2+</sup> extrusion occurs via Na<sup>+</sup>/Mg<sup>2+</sup> exchanger, were the basis of the experimental demonstration that human *SLC41A1* gene encodes for the Na<sup>+</sup>/Mg<sup>2+</sup> exchanger [18].

Mg<sup>2+</sup> extrusion can also occurs by cAMP-independent mechanisms following  $\alpha$ 1-adrenergic stimulation, since it is reported that  $\alpha$ 1-adrenergic receptor-mediated Mg<sup>2+</sup> extrusion in perfused livers and isolated hepatocytes, requires an increase in cytosolic Ca<sup>2+</sup> concentration and the activation of Ca<sup>2+</sup>/calmodulin intracellular signaling [62]. This mechanism evidences the linking between Ca<sup>2+</sup> signaling and Mg<sup>2+</sup> homeostasis.

### 1.3.2 Mg<sup>2+</sup> accumulation

The mechanisms that regulate magnesium accumulation inside the cells are still largely unknown. The main pathway for Mg<sup>2+</sup> uptake in mammalian cells is the activation of protein kinase C (PKC) signaling. Several research groups have

provided evidence about the supporting role of PKC in mediating  $Mg^{2+}$  accumulation [63].

The linking between PKC activation and  $Mg^{2+}$  accumulation is further corroborate by the observation that  $Mg^{2+}$  uptake does not occur under condition in which cells are treated with known inhibitors of PKC, for example staurosporines [64]. However, several lines of evidence indicate that other pathways are involved in the regulation of  $Mg^{2+}$  entry such as MAPKs and EGF signaling [65]. Indeed, the inhibition of MAPKs signaling hampers  $Mg^{2+}$  entry and blocks cell cycle progression by affecting cyclin activity, while EGF controls the TRPM6 channel expression in the apical domain of renal epithelial cells and the consequently  $Mg^{2+}$  reabsorption [66]. Indirect evidence of  $Mg^{2+}$  homeostasis regulation by EGF is provided by the induced  $Mg^{2+}$  wasting and hypomagnesemia following by the use of antibodies against EGF for the treatment of several form of colon cancer [67], [68].

## **1.4 Magnesium and Cell Proliferation**

Compelling evidences show that magnesium content is directly correlated to proliferation. The articulated phenomenon of cell proliferation begins following the binding of hormones or growth factors to their specific surface receptor. As a consequence, the mitotic signals start a phosphorylation-based signal cascade which leads to the activation of transcription factors crucial for the protein synthesis, which is required for the initiation of DNA synthesis and mitosis.

Mg might reasonably be involved in every single step of the mitogenic stimuli: from receptor-mediated mitotic signals and transphosphorylation reactions to gene transcription and protein synthesis occurring prior to cell division [69]. Moreover, key enzymes of DNA duplication, as polymerase and ligases, required  $Mg-ATP^{2-}$  for their activity, and finally Mg is involved in the cytoskeleton re-arrangement leading to the formation of the mitotic spindle and cytokinesis [70].

The plethora of functions that magnesium carry out on cell proliferation regard also the stabilization of DNA structure and regulation of the opening/closing of ion channels for the change of pH and calcium concentration prior to cell division (Fig. 1.2).

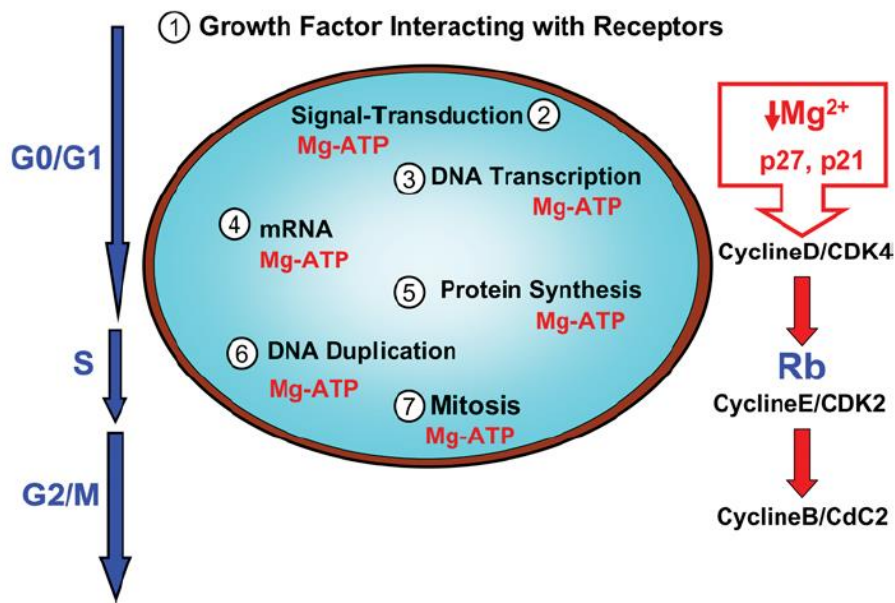


**Figure 1.2: Pathway of cell proliferation and its regulation by magnesium** [71]. All step leading to cell proliferation, from signal transduction to mitosis, may be affected by magnesium availability. At the molecular level, low Mg up-regulates p27 and p21 inhibitory proteins, leading to cell cycle arrest through inhibition of cyclin/CDK complexes and consequent inhibition of the Rb (retinoblastoma)-regulated restriction point (Taken from Wolf et al, 2008).

Experimental evidence clearly indicates that growing cells contain more Mg than resting ones [72], coherently with the promoting role of Mg<sup>2+</sup> on protein and DNA synthesis.

However, the dependence of growth rate to extracellular magnesium availability vary from the different cellular types analyzed. In general, normal diploid cells are highly sensitive to changes in magnesium availability: endothelial cells and fibroblasts decreased their growth rate to a considerable extent when the cells were maintained in 0.1 mM extracellular Mg<sup>2+</sup> [73], [74]. Conversely, immortalized cells, showed a 50% growth inhibition only upon exposure to 0.05 mM Mg<sup>2+</sup> [75], while tumour cells, as for example HL60 leukaemia cells, proved to be the most resistant ones, showing an unaltered growth rate at 0.05 mM extracellular Mg<sup>2+</sup> [76].

Furthermore, it has been shown that incubation of cells in low magnesium concentrations causes growth arrest, resulting in an increased percentage of cells in G0/G1 phase, a decrease percentage of cells in S phase and, occasionally, a slightly

increased percentage of cells in G2/M phase [77]. However, the re-addition of  $Mg^{2+}$  caused a rapid and relevant rise in the proliferating rate, suggesting that cell cycle arrest is reversible [78]. At the molecular level, low Mg availability trigger the up-regulation of the cell cycle inhibitor p27 [75] and p21 [79]. In parallel, cyclins D and F, which promote cell cycle progression, decrease [80].

On the contrary increasing the amount of extracellular  $Mg^{2+}$  induces activation of cell cycle, which is trigger by MAP kinases protein, leading to up-regulation of cyclins D and F and decreased expression of p21 and p27 [66].

These findings suggest that  $Mg^{2+}$  availability affects cell cycle by influencing the transcription of the cell cycle regulatory proteins such as p21 and p27, cyclins and CDKs.

Harry Rubin postulated the theory of “Membrane Magnesium Mitosis”, suggesting that cytoplasmic free  $Mg^{2+}$  is the unifying regulatory element of cell growth and proliferation. On the basis of this theory, membrane perturbations induced by growth factors causes a decrease of  $Mg^{2+}$  binding affinity for negatively charged membrane sites and result in increased intracellular  $Mg^{2+}$  levels, which triggers in turns protein synthesis and a number of  $MgATP^{2-}$  dependent reactions. The products of these reaction further enhanced protein synthesis and the related DNA synthesis, ultimately leading to cell division [81], [82].

## **1.5 Magnesium and Cell Differentiation**

While clear evidence has been provided about the relevance of magnesium in driving cell proliferation, little is known about its involvement to the modulation of cell differentiation [83]. Data presents in literature are relatively few and discordant. Differentiation is an extremely complex framework governed by numerous and different factors as receptor-mediated stimuli, growth inhibitors, contact inhibition, intercellular junctions. Moreover, it requires the activation of cell-specific genetic programs that can be differentially affected by Mg [84].

As regard the consequence of Mg restriction, some studies described that low extracellular magnesium promotes cell differentiation, while others reach opposite

conclusions. It is reported that Mg deficiency reversibly antagonized the differentiation of HL60 cells exposed to differentiating agents such as DMSO and retinoic acid [76], [85] and akin to these observations it was also found that Mg restriction retards phorbol ester-induced differentiation in U937 cells [83]. In contrast to the above findings, it has been shown that Mg-restricted media rapidly reversed the transformed phenotype of fibroblasts [86], and in C2C12 myogenic cells, Mg deficiency upregulated Myod, one of the transcription factors fundamental for myogenesis [87].

Moreover, also the exposure to high extracellular Mg has provided discordant results. It was observed that excessive extracellular Mg blocks pre-osteoblast differentiation [88] and inhibits matrix mineralization in the prechondrogenic cell Line ATDC5 [89], while in U937 high extracellular Mg accelerates cell differentiation [83].

In pancreatic islet RINm5F cells, both low and high extracellular Mg impaired insulin synthesis without altering cell morphology, suggesting that in this cells the effects of Mg may be confined to the induction of functional rather than morphologic differentiation [90].

Again, different results were obtained in endothelial cells and pre-adipocytes where differentiation seems to be independent from extracellular Mg [83].

Together, these findings suggest that fundamental differences exist between various cell types in the contribution of Mg to cell differentiation. The relationship between Mg and cell differentiation thus remains open to debate and further experimental evidences are certainly needed to shed new light on this issue.

## **2 TECHNIQUES TO MEASURE MAGNESIUM**

### **2.1 Introduction**

Although the biological relevance of magnesium is now widely recognized, a full understanding of cellular magnesium homeostasis has not been achieved. This can partly be attributed to the lacking of available techniques and methodologies able to rapidly and accurately measure changes in cellular Mg content. Furthermore, mammalian cells tightly regulate magnesium ion content through specific mechanisms controlling  $Mg^{2+}$  entry and efflux across the cell membrane and the membrane of various cellular organelles, as well as intracellular  $Mg^{2+}$  buffering under resting condition, and following hormonal and metabolic stimuli [91]. Indeed, magnesium buffering within the cytoplasm at concentration in the sub-millimolar range implying that  $Mg^{2+}$  fluctuations could only be traced by techniques able to sense minor changes [92].

### **2.2 Principle techniques to determine magnesium**

Flame Atomic Absorption Spectroscopy (F-AAS) has been historically the first and most common approach to assess total cellular magnesium in cell or tissue acidic extracts. Even if is still considering the reference technique for the quantification of the total intracellular magnesium, it requires large samples (at least millions of cells or several milligram of tissue). Other more sensitive techniques require smaller sample sizes, such us Inductively Coupled Plasma Mass Spectroscopy (ICP-MS) and Graphite Furnace AAS (GF-AAS). These techniques indubitably offer improved detection limits, however require instrumentations not easily available in any laboratory, more complex analytical procedures and specific technical skills and competencies [1][2]. Moreover, the major limitation of all these methods is that magnesium free and bound forms cannot be discriminated and information about intracellular distribution in whole cells can only be derived indirectly by cell permeabilisation or subcellular fractioning [92].

On the other hand, free  $Mg^{2+}$  can be measured from the chemical shift of the Mg-ATP peak by  $^{31}P$  Nuclear Magnetic Resonance (NMR) spectroscopy [95], [96], by electron probe microanalysis [97], and by ion-selective microelectrodes [98]. All these techniques have different fields of application, depending on the cells or tissues studied, but they all present serious limitations.

In particular,  $^{31}P$  NMR relies on the fact that most magnesium in the cytosolic matrix is bound to ATP. Therefore, variation in the acquired chemical shift associated to the phosphorylated molecule present in the cytoplasm including Inorganic Phosphate (Pi), Phosphocreatine (PCr) and ATP depends on the  $Mg^{2+}$  concentration [99].

$^{31}P$  NMR allows an accurate measurement of cytosolic free  $Mg^{2+}$  in vivo but supplies no information on the total magnesium concentration and its distribution among cellular subcompartments.

Magnesium content in different subcellular compartments can be evaluated by electron probe microanalysis in freeze-died cryosections. This technique is invasive and again does not provide information on free and bound  $Mg^{2+}$  and does not allow kinetic measurements of  $Mg^{2+}$  fluxes [100]. At last, ion-selective microelectrodes allow direct measurement of free  $Mg^{2+}$  in single cells or plasma, but this technique discloses problems of interference with other ions (Ca, K), requires very large amount of cells for intracellular measurement and is a method technically difficult in single cells [101].

Considering the serious limitation of the available techniques, suitable tools for studying the role of magnesium in cell processes require the ability to monitoring the dynamics of its concentration in living cells with both spatial and temporal resolution.

Recently, fluorescent probes have been widely used as tools for the dynamic measurement of ion distribution and concentration in cells [102]. They are highly sensitive and offer imaging by fluorescent microscopy in an easier and less cell damaging way than other methods (e.g. ion-selective electrodes, NMR techniques) [103].

In this context, fluorescent probes, thanks to their sensitivity, represent the method of choice to detect even minor changes in ion concentration.

## 2.3 Fluorescent chemosensors

Chemical sensing using fluorescence to signal a molecular recognition event was first shown by Tsien et al. in the early 1980s reporting the synthesis of the first fluorescent calcium indicators [104], [105]. The typical structure of a fluorescent dye consists of two moieties: a receptor responsible for the molecular recognition of the analyte, and a fluorophore, which signals the recognition event [106].

Although the importance of  $Mg^{2+}$  is now widely acknowledged, for the past five decades, all the efforts in developing fluorescent probes have been made to study and monitor  $Ca^{2+}$  concentration in vivo, as a fast-acting principal second messenger. Therefore,  $Mg^{2+}$  has become the “forgotten cation” and the first  $Mg^{2+}$  indicators were simply derived from  $Ca^{2+}$  probes [92].

Indeed, these first probes exploited the property of APTRA (o-aminophenol-N,N,O-triacetic acid) and its fluorinated derivatives, which are structural analogues of the  $Mg^{2+}$  chelator EDTA (ethylenediaminetetraacetic acid) [107]. The APTRA structure was then modified around the furan ring, resulting in the fluorescent indicator FURAPTRA (mag-fura-2) which is still used in many laboratories [11].

Since then, many other dyes selective for  $Mg^{2+}$  have been synthesized, and most of them are analogues to the corresponding  $Ca^{2+}$  probes such as, mag-fura-2 (FURAPTRA, analogue of fura-2), mag-indo-1 (analogue of indo-1), mag-fluo-4 (analogue of fluo-4) and magnesium green (analogue of calcium green).

These are the commercial dyes most widely used in tracking and quantifying the intracellular ion Mg concentration. However, they are all characterized by  $K_d(Mg^{2+})$  values in the millimolar range: therefore, they are suitable to detect mainly cytosolic magnesium ions (only 5% of the total) without providing any information about the bound pool. In addition, since they are derived from  $Ca^{2+}$ -specific probes, they retain a considerable affinity for this ion and massive changes in  $Ca^{2+}$  concentrations may interfere with  $Mg^{2+}$  assessment.

## 2.4 Last generation fluorescent probes

The limitations of the commercial probes mentioned above prompted the scientific community to develop new magnesium fluorescent indicators exploitable in live cells, which has resulted in the synthesis of several novel dyes with improved characteristics such as more affinity, selectivity and specificity towards Mg [92].

### 2.4.1 The KMG series

The need to optimized magnesium sensors, especially in terms of binding affinity, led to the synthesis of KMG derivatives. The molecular design of these compounds is based on a charged  $\beta$ -diketone binding site and a coumarin fluorophore that has a strongly improved magnesium selectivity. The first molecule of the series, KMG-20 [108], achieved better selectivity for  $Mg^{2+}$  ( $k_d$  10 mM) in comparison to commercial probes, but the choice of a coumarin as chromophore provide an excitation in the UV region which prevent the excitation by the Ar<sup>+</sup> laser commonly used with a confocal microscope [103]. KMG-104, which has a fluorescein chromophore, is an up-to-date version of the KMG series of magnesium probes, with improved properties and a  $K_d$  for  $Mg^{2+}$  of 2.1 mM [109]. KMG-104 can be excited in the visible range and its selectivity for  $Mg^{2+}$  over  $Ca^{2+}$  is much better than that displayed by commercial probes, rendering these dyes completely insensitive to physiological changes in cytosolic  $Ca^{2+}$  concentration. Moreover, KMG-104 was used to detect cytosolic  $Mg^{2+}$  accumulation upon mitochondria depolarization, which led to the hypothesis that mitochondria could be intracellular magnesium stores [109]. These characteristics make KMG-104 one of the most promising alternatives to detect free  $Mg^{2+}$  by live cell imaging.

Another member of the family is the molecule KMG-301, an  $Mg^{2+}$ -selective fluorescent probe that is functional in mitochondria. It is composed by a rhodamine skeleton as the chromophore and by a charged- $\beta$ -diketone moiety as the binding site for  $Mg^{2+}$ . Indeed, this probe changes its fluorescence properties solely depending on the  $Mg^{2+}$  concentration in mitochondria under physiological condition [110]. Moreover, combining measurements of KMG-301 together with KMG-104, the derivatives specific for cytosolic  $Mg^{2+}$ , it make possible the comparison of the  $Mg^{2+}$

dynamics in the cytosol and in mitochondria under mitochondrial uncoupling conditions in PC12 cells (rat pheochromocytoma of the adrenal medulla) and in hippocampal neurons [110].

More recently another very promising  $Mg^{2+}$  selective fluorescent probe, KMG-104-AsH [111] was developed by combining the dye KMG-104 [112] and the fluorescent probe for protein-labeling, "FlAsH" that fluoresces only when it binds specifically to a TC-tag peptide genetically added to target proteins. KMG-104-AsH only becomes fluorescent when binding to both the TC-tag and  $Mg^{2+}$ . Application of the probe for imaging of  $Mg^{2+}$  in HeLa cells showed that this KMG-104-AsH is membrane-permeable and binds specifically to tag proteins, such as TCTag-actin and mKeima-TCTag targeted to the cytoplasm and the mitochondrial intermembrane space. Therefore, this probe was shown to be useful for localized molecular imaging of changes in  $Mg^{2+}$  concentration and hence for elucidating the dynamics and mechanisms of intracellular localization of  $Mg^{2+}$  [111].

#### **2.4.2 KCM-1**

KCM-1 is a novel single-molecular multianalyte sensor which permitted the simultaneous imaging of intracellular  $Ca^{2+}$  and  $Mg^{2+}$  in a cell [112]. The new dye combines in a single molecule a coumarin moiety as a stable fluorophore excitable with visible light, BAPTA as the  $Ca^{2+}$ -selective binding site and a charged  $\beta$ -diketone as the  $Mg^{2+}$ -selective binding site. As a consequence, fluorescence emission of KCM-1 shows a spectral blue shift upon complexation to  $Ca^{2+}$  and a red shift in the presence of  $Mg^{2+}$ . The use of a single probe that allows the sensing of multiple analytes with different spectral responses is a promising way to overcome the difficulties encountered when loading multiple indicators. Despite the novelty represented by a single-molecular multianalyte sensor, the binding characteristics of KCM-1 are quite inadequate, since the  $K_d$  values for  $Ca^{2+}$  and  $Mg^{2+}$  are reported to be 14  $\mu$ M and 26 mM respectively, which are definitely too high to actually measure the intracellular concentrations of these ions. However, KCM-1 has been capable to detect distinct  $Ca^{2+}$  and  $Mg^{2+}$  transients upon mitochondrial depolarization [112].

### 2.4.3 AMg1 e AMg1-AM

AMg1 is a novel Mg indicator specifically designed for two-photon microscopy.

AMg1 was designed with 2-acetyl-6-(dimethylamino)naphthalene as the two-photon chromophore and APTRA as the Mg<sup>2+</sup>-selective binding site [113].

To enhance the cell permeability of the probe, the carboxylic acid moieties were converted into acetoxymethyl (AM) esters (AMg1-AM).

Moreover, increasing the polarity of the solvent, the esterified form of the probe (AMg1-AM) presents an high shift of fluorescence toward red, which allows to discriminate between the cytosolic hydrolysed form of the probe (red fluorescence) and the membrane-associated form (blue fluorescence).

This characteristic should allow to discriminate the contribution of membrane-bound probe, and thus eliminate a source of error in Mg<sup>2+</sup> quantification [113].

### 2.4.4 The DCHQs series

Despite the growing interest in the synthesis of new and more specific chemosensors for magnesium, all the last generation fluorescent probes mentioned above still have a  $K_d(\text{Mg}^{2+})$  in the millimolar range. The lack of selective and specific compounds for total magnesium currently represents a technical limitation in the study of intracellular content and distribution of this cation [114]. Indeed, a large body of experimental evidence documenting the occurrence of large fluxes of Mg<sup>2+</sup> across the cell membrane in response to a variety of hormonal and metabolic stimuli, attended by considerable changes in plasma Mg<sup>2+</sup> levels [15]. These fluxes, however, have resulted in relatively small changes in free Mg<sup>2+</sup> intracellular concentration, even though significant changes in total Mg content within cells have been observed [91].

This suggest that the amount of free Mg<sup>2+</sup> is kept constant at the level necessary for cellular metabolic demands by the ability of the cell to rapidly buffering modification of the free fraction, suggesting that modification of magnesium availability are accomplished by changes in the distribution (binding) of magnesium among cellular subcompartments [76], [12]. In this perspective, a tool able to detect and/or

discriminate between free and total magnesium and between  $Mg^{2+}$  content of cytosolic and intracellular subcompartments would be particularly useful [115].

8-Hydroxyquinoline (8-HQ), is considered as the second  $Mg^{2+}$  chelating agent in importance after EDTA [116]. 8-HQ is mostly non-fluorescent in aqueous or organic solutions and undergoes a fluorescence enhancement upon cation binding, which results in an intense yellow-green signal. Furthermore, the fluorescence of the complex species depends on the environment and becomes higher as lipophilicity increases [117], [118]. The selectivity of 8-HQ is poor, but it can be improved by appropriate substitution. In this context, particular interest has gained a new family of fluorescent molecules obtained by conjugation of a diaza-18-crown-16 with two 8-hydroxyquinolines bearing various substituents (DCHQs) (Fig 2.1) [92].

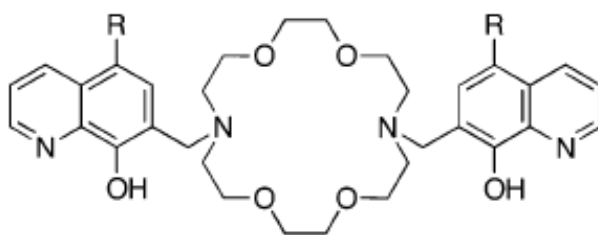


**Figure 2.1: Chemical structure of the DCHQ-based probes**

These molecules have been proposed as effective chemosensors for different ions; in particular, some members demonstrated high specificity for  $Mg^{2+}$ , with an excitation wavelength around 363 nm and an emission wavelength centered around 505 nm.

DCHQ1, the first member of the family, binds  $Mg^{2+}$  with much higher affinity than any other available probe ( $K_d = 44 \mu M$ ) and shows a strong fluorescence increase upon complexation. Remarkably, its fluorescence is not significantly affected either by other divalent cations, most importantly  $Ca^{2+}$ , or by pH changes within the physiological range [29] [33]. It is worth noting that DCHQ-based compounds proved to be a valuable tool to detect total cell magnesium, due to their  $K_d$  in the

micromolar range, that is the same order of magnitude as (and hence able to compete with) ATP, which is the major intracellular  $Mg^{2+}$  ligand [114], [120].

Moreover, DCHQ1 readily permeates cells, binds intracellular  $Mg^{2+}$ , and it has been employed to map intracellular ion distribution and movements in live cells by confocal imaging [114], [115].

Furthermore, this probe has been shown to be a suitable analytical tool capable to quantitatively assess the total intracellular magnesium in different cell lines [120]. The evaluations of cell total magnesium by DCHQ1 fluorescence in leukemic (HL60) and mammary epithelial (HC11) cells resulted in a three to fourfold overestimation compared to magnesium measured by AAS. The hydrophobic nature of DCHQ1 and the lifetime measurements performed by single-photon counting spectrofluorometry, suggested that the enhancement obtained in intact cells could be due to the entrapment of the probe in membrane compartments [115]. Indeed, it has been described that hydrophobic derivatives of hydroxyquinoline preferentially distribute into lipophilic moieties [121]. Farruggia et al. showed that upon disruption of cells by sonication, DCHQ1 fluorescence substantially decreases, obtaining overlapping results with AAS by using a simple spectrofluorimetric assay [115] [120].

Besides the unquestionably analytical value of DCHQ1, some limitations of this probe, such as its poor intracellular retention and the fact that it can be excited only in the UV region, have restricted its application for monitoring magnesium movements across intracellular compartments. Farruggia et al. developed a new method for the chemical synthesis of DCHQ compounds based on microwave heating, in order to reduce the reaction time, to increase the yield and to minimize the side reactions. This approach ultimately results in much easier purifications and higher quality products compared to the classic synthetic approach [122]. Moreover, the new protocol has permitted to easily modify the basic structure of DCHQ1 by introducing various functional groups in position 2, 4 or 5 of the quinolone ring system [122]. New compounds were designed to overcome the aforementioned limitations of the parent probe and to improve fluorescence response upon cation binding, uptake and intracellular localization preventing the unique feature of selectively binding total intracellular magnesium [114]. Among

the panel of the DCHQ derivatives, particularly interesting features were observed for the derivative bearing a phenyl group as a substituent in position 5' of each hydroxyquinoline arm, named DCHQ5 (Fig. 2.2).

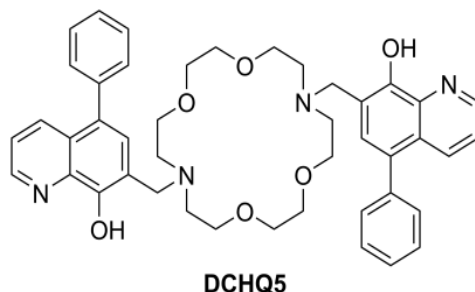


**Figure 2.2: Chemical structure of the DCHQ5**

In fact this probe presents improved characteristics compared to DCHQ1 such as higher fluorescence, membrane staining, a much higher retention within loaded cells and the possibility to avoid the UV excitation, which could be potentially cytotoxic, as DCHQ5 could be excited both in the UV and visible spectrum range [114]. For all these peculiar features, DCHQ5 appears to be a valuable candidate to shed new light on magnesium homeostasis at the cellular level.

#### **2.4.5 MagFRET**

Last development in the field of fluorescence chemosensors is referred to the genetically encoded metal sensors based on the Förster Resonance Energy Transfer (FRET). Indeed, genetically encoded fluorescent sensor proteins provide an attractive alternative to small-molecule fluorescent sensors, because they do not require cell-invasive procedures, their concentration can be tightly controlled and they can be targeted to different locations in the cell [123].

MagFRET-1 is the first genetically encoded fluorescent magnesium sensor with a  $K_d$  for  $Mg^{2+}$  of 148  $\mu M$ , and it shows a 50% increase in emission ratio upon  $Mg^{2+}$  binding [124]. A general advantage of genetically encoded sensors is that their subcellular localization can be easily controlled, and in situ experiments in HEK293 cells showed that MagFRET-1 could be targeted to the cytosol and the nucleus. As regard

the limitation of MagFRET-1, although it is responsive to changes in  $Mg^{2+}$  concentration in permeabilized cells, for some unknown reason MagFRET-1 is less responsive in intact cells. Moreover, MagFRET-1 responds to changes in  $Mg^{2+}$  concentration in the order of seconds both in vitro and in cells, but as the other protein-based sensors, it displays slower kinetics than small molecule sensors and for this reason, it is not able to detect extremely fast  $Mg^{2+}$  movements. In addition, MagFRET-1 miss sensitivity for changing in overall  $Mg^{2+}$  levels over longer periods of time [124].

## 2.5 X-Ray microscopy

In recent years, growing interest has been given to single cells analysis for investigating the smallest dimensions of living systems.

The requirement of elemental analysis in biological system is a challenging issue for defining the intracellular concentration map of a given element. Indeed, the biological function of a chemical element in cells does not only require the determination of its intracellular quantity, but also the spatial distribution of its concentration, since the different localization of a specific element within a cell often refers to a different biological function.

Moreover, many basic aspects and regulatory mechanisms of cell functions are related to the intracellular compartmentalization of the ions whose different gradient concentrations generate the driving force of many cellular processes [125]. Further insights into biological processes and cellular analysis require quantitative techniques, mainly nondestructive with high elemental and chemical sensitivity and high spatial resolution. Nowadays, several quantification techniques, based on electron, photon, and synchrotron X-ray and ion, allow to obtain the elemental and chemical imaging of single cells [126].

Among these, X-Ray microscopy based on synchrotron light source has gained increasing attention in the last years thanks to its extreme sensitivity and to the improvements that have been achieved in third-generation Synchrotron X-ray sources and in X-ray focusing optics. In particular, X-ray Fluorescence Microscopy (XRFM) is a highly sensitive method for mapping elements distribution in single

cells at nanoscale resolution [127]. However, when applied to whole cells, the fluorescence intensity map obtained with XRFM can be misleading because it gives information on the total element content and not on element concentration, as the probed volume is not known [128]. Indeed, biological samples are by definition heterogeneous in density and thickness; therefore, in order to be quantitative, XRFM must be complemented with other imaging techniques able to provide detailed density and volumetric intracellular distribution [126].

Towards this end, extremely interesting is a new methodology for quantitative mapping of light elements in cells, based on combination of compositional and morphological information, derived respectively by X-ray Fluorescence Microscopy (XRFM), Atomic Force Microscopy (AFM) and Scanning Transmission X-ray Microscopy (STXM) [125]. In particular, authors shown that the combination of AFM with STXM allows to retrieve the intracellular density. Thus, combining the density obtained with STXM and AFM to the fluorescence intensity map derived by XRFM, it is possible to obtain high resolution molar concentration and mass fraction maps of fundamental life elements (Carbon, Nitrogen, Oxygen) as well as light metals, in particular Mg [125]. By using the principles of this technique, a new developed method allows to address Magnesium in subcellular compartments.

### 3 AIMS

Although the biological relevance of magnesium is now widely recognized, a full understanding of cellular magnesium homeostasis and the mechanisms regulating its distribution and intracellular compartmentalization have not been achieved. This can partly be attributed to the lacking of available techniques and methodologies able to rapidly and accurately measure changes in intracellular Mg content [92]. Mammalian cells tightly regulate magnesium ion content through specific mechanisms controlling  $Mg^{2+}$  entry and efflux across plasma membrane and other membrane of sub-cellular organelles [91]. Indeed, magnesium buffering within the cytoplasm at concentration in the sub-millimolar range implies that  $Mg^{2+}$  fluctuations could only be traced by techniques able to sense minor changes [92]. Moreover, free and total magnesium undergo different and independent regulatory mechanisms, and it is reported that modifications of magnesium availability biologically relevant are accompanied by major changes in total Mg content, while the free fraction is well buffered, indicating that rearrangements took place in the distributions of bound magnesium among cellular ligands and/or sub-compartments [12], [76].

In this perspective, notably appealing are the members of the fluorescent dyes diaza-crown-hydroxyquinoline family which demonstrated high specificity for  $Mg^{2+}$  having a  $K_d$  in the micromolar range [115] making these probes able to detect total intracellular magnesium.

Among these, particularly interesting features were observed for the phenyl derivative of these family (DCHQ5) that showed high response to cation binding, membrane staining, high intracellular retention and the possibility to be excited both in the UV and visible spectrum range [114].

Taking into account the peculiar properties of DCHQ5, in the first part of the project we investigated the analytical capabilities of this fluorescent probe for the quantitative assessment of total intracellular magnesium content and its biological applications. To accomplish this task, we performed a comparative study of DCHQ5 and DCHQ1, the latter being the mother probe of the series which showed preliminary encouraging results comparable to atomic absorption spectroscopy [120]. We performed fluorescence spectroscopy assays to evaluate the fluorescence

intensity and stability of the two probes, and also flow cytometry analyses in viable cells to test intracellular retention of DCHQ1 and DCHQ5, as well their fluorescence stability over time. Moreover, we deeply investigate the analytical performances of the probes for the quantitative assessment of the intracellular total magnesium by using a new spectrofluorimetric protocol based on a standard titration curve in sonicated cellular samples. For these analyses we used AAS as gold standard, and we also estimated the sensitivity of our method by the evaluation of the limit of detection.

The unique feature of DCHQ5 to be excitable in the visible region renders this dye very interesting for fluorescence lifetime imaging (FLIM) applications. In fact, this property allows to minimize the background interference coming from the cell autofluorescence. In addition, a common characteristic of the members of the DCHQ family is to show a bi-exponential fluorescence lifetime decay in the intracellular environment [115]. Therefore, we also performed FLIM measurements in collaboration with the group of Professor Paola Taroni at the Politecnico of Milan to explore the capability of DCHQ5 to obtain FLIM image of intracellular Mg which has never been done so far.

Moreover, DCHQ5 was also exploited for studying the involvement of magnesium in the commitment of human adipose-derived mesenchymal stem cells (hASCs) with a mixture of hyaluronic, butyric and retinoic (HBR) acids, in collaboration with the research group of Professor Carlo Ventura. In particular we monitored the intracellular total magnesium content of hASCs cultured in complete and also in Mg-free medium. In parallel, we also performed cell cycle analysis and we examined the gene expression of a panel of markers representing the multilineage potential of these cells. Finally, the gene expression was assessed again after the re-addition of Mg to the deprived medium to further investigate the possible Mg modulation on gene expression.

The second part of this research was aimed at comparing single cells elemental analysis performed with synchrotron-based fluorescence and cell population analysis carry out by DCHQ5. In particular, we investigated the pitfalls and advantages of the two different strategies for the quantification of intracellular Mg

in three cellular models: human colon carcinoma cells sensitive (LoVo S) and resistant (LoVo R) to doxorubicin, endothelial cells isolated from the umbilical vein (HUVEC) wild type and genetically engineered to silence TRPM7, and human SaOS2 bone osteosarcoma cells cultured in standard and Mg-deprived conditions.

We exploited a standard-less approach providing a complete characterization of whole single-cells by combining X-Ray Fluorescence Microscopy (XRFM), Atomic Force Microscopy (AFM) and Scanning Transmission X-ray Microscopy (STXM). This method allows the quantification of the intracellular spatial distribution and total concentration of magnesium and other light elements (C, O, N) in whole dehydrated cells [125]. Subsequently, we quantified the total amount of intracellular  $Mg^{2+}$  in a large population of the same samples by using DCHQ5 probe and spectrofluorimetric technique, aimed to compare the data obtained in small groups of dehydrated cells with ones of a large cell population. Moreover, the data obtained by synchrotron-based single cell analysis were normalized for the volume of the corresponding population to further compare the concentration calculated in single cells analysis with the concentration calculated using DCHQ5.

## 4 MATERIALS AND METHODS

### PART I

#### 4.1 Reagents

All reagents were from Sigma Aldrich (Italy), if not differently stated, and were of ultrapure grade. Dulbecco's Phosphate-Buffer Saline (DPBS) was purchased without  $\text{Ca}^{2+}$  and  $\text{Mg}^{2+}$ . The fluorescent probes were dissolved in dimethyl sulfoxide (DMSO) to a final concentration of  $1 \text{ mg mL}^{-1}$  (DCHQ1  $1.7 \text{ mM}$ , DCHQ5  $1.4 \text{ mM}$ ). Aliquots were kept at  $4^\circ\text{C}$  in the dark.

Fetal bovine serum (FBS) was stripped of Mg by dialysis, using a dialysis membrane (Medicell International LTD, UK) with a 3500 D cut-off against Puck buffer ( $\text{NaCl}$   $800 \text{ g/L}$ ,  $\text{KCl}$   $4 \text{ g/L}$ ,  $\text{NaHCO}_3$   $3.5 \text{ g/L}$ , D-glucose anhydrous  $5 \text{ g/L}$ , pH 7.4) plus EDTA  $1 \text{ mM}$  for two days, and Puck buffer alone for the last three days. The Ca content in dialysed FBS was restored by adding  $\text{CaCl}_2$  at a final concentration  $1.8 \text{ mM}$ . The FBS was then sterilized by filtering through a  $0.45 \text{ }\mu\text{m}$  filter.

Mg-free MEM was purchased from Invitrogen (San Giuliano M.se, Italy). To reconstitute the full magnesium medium content  $\text{MgCl}_2$   $1 \text{ mM}$  was added.

#### 4.2 Cell culture

All the following cell lines (human HL60 Promyelocytic Leukemia, human HT29 colon adenocarcinoma, human LoVo colon adenocarcinoma, human U2OS and SaOS2 osteosarcoma) were grown at  $37^\circ\text{C}$  and  $5\% \text{ CO}_2$  in RPMI 1640 medium, supplemented with  $2 \text{ mM}$  L-Glutamine,  $10\%$  heat-inactivated fetal bovine serum (FBS),  $100 \text{ units mL}^{-1}$  penicillin and  $100 \text{ }\mu\text{g mL}^{-1}$  streptomycin.

##### 4.2.1 Adipose- derived stem cell isolation

According to the policy approved by the local ethical committee, all tissue samples were obtained after informed consent from healthy donors. Human subcutaneous adipose tissue samples were obtained from lipoaspiration/liposuction procedures from several regions of the body, such as hip, thigh and abdominal regions, and

collected into a sterile container. After washing, lipoaspirates were digested with 0.2% collagenase A type I solution (Sigma-Aldrich), under gentle agitation for 45 min at 37°C, and centrifuged at 650 *g* for 10 min to separate the stromal vascular fraction (SVF) from adipocytes. If necessary, the SVF fraction was treated with red blood cell lysis buffer for 5 min, and then centrifuged again. The supernatant was discarded and the cell pellet was resuspended and seeded in culture flasks in Minimum Essential Medium Eagle - Alpha Modification ( $\alpha$ -MEM, Lonza) supplemented with 20% heat-inactivated fetal bovine serum (FBS), 1% penicillin-streptomycin, 2 mM L-glutamine, and incubated at 37°C in a humidified atmosphere with 5% CO<sub>2</sub>. When the cultures were near confluence, the cells were detached by treatment with trypsin-EDTA solution (Sigma-Aldrich), characterized, subcultured, and used at passage 3-6.

#### **4.2.2 Adipose- derived stem cell treatment**

Twenty-four hours after seeding in  $\alpha$ -MEM 10% FBS, cells were cultured in absence (Ctr) or presence (HBR) of a mixture of hyaluronic (1 mg/ml), butyric (5 mM) and retinoic acid (1  $\mu$ M), referred as HBR. The day of treatment is considered time 0 of analysis. The culture basal medium of all experiments was the Mg-free MEM (Invitrogen) for studying the effect of Mg deprivation to hASCs commitment (referred as -Mg). For the experiment in presence of normal Mg concentrations, the Mg-free MEM medium was supplemented with MgCl<sub>2</sub> 1mM.

For Mg-free media, dialysed FBS was used.

#### **4.3 Photophysical measurements**

Absorption spectra were recorded on a Perkin-Elmer Lambda 45 spectrophotometer. Absorption spectra of DCHQ1 25 $\mu$ M were acquired in two different buffer: MeOH:MOPS (methanol:H<sub>2</sub>O 1:1 buffered at pH 7.4 with 3-morpholinopropane-1-sulfonic acid at room temperature) and DPBS upon addition of increasing amount of MgSO<sub>4</sub> (from 0 to 500  $\mu$ M). Absorption spectra of DCHQ5 10  $\mu$ M were acquired in MeOH:MOPS.

For the fluorescence spectroscopy measurement, uncorrected emission and corrected excitation spectra were obtained with a PTI Quanta Master C60/2000 spectrofluorimeter (Photon Technology International, Inc., NJ, USA).

#### **4.4 Titration of Mg<sup>2+</sup> binding by fluorescence spectroscopy**

Increasing amount of a 100 mM solution of MgSO<sub>4</sub> were added to a 25 μM solution of DCHQ1, in two different buffer (DPBS and MeOH:MOPS), and to a 10 μM solution of DCHQ5 in MeOH:MOPS, to obtain Mg<sup>2+</sup> concentration from 0 to 500 μM. Fluorescence spectra were recorded, upon excitation at 360 nm, in the range from 400 to 650 nm.

#### **4.5 Stability of the probes**

For the determination of the stability of the probes, the emission wavelength was set to the value of the maximum (500 nm for DCHQ1 and 510 nm for DCHQ5) and the samples were excited continuously for 30 minutes. Spectra were acquired at two different concentrations of magnesium, chosen to test a Mg:dye ratio of 1:2 and 100:1.

#### **4.6 Quantification of total cell magnesium by AAS**

Total magnesium content was assessed by AAS on acidic cellular extracts of a sample of 1-2 x 10<sup>6</sup> cells/mL. Harvested cells were washed twice in cold DPBS by centrifugation and then pelleted at 250 *g*. Ion extractions were obtained by overnight treatments of the cell pellets with 3 mL of 1.0 N HNO<sub>3</sub>. After agitation and centrifugation of samples, magnesium was assayed on cell supernatants by AAS (Instrumentation Laboratory mod. S11, USA or Perkin Elmer AA200) equipped with an air/acetylene flame.

#### **4.7 Quantification of total cell magnesium by a spectrofluorimetric assay**

Total magnesium content was assessed on sonicated cell samples by the two fluorescent dye DCHQ1 and DCHQ5 choosing a method that involves the

construction of a standard curve. Briefly, DCHQ5 was dissolved to a final concentration of 15  $\mu\text{M}$  in a mixture which contains 10% of DPBS in a solution 1:1 of MeOH:MOPS 2 mM (pH 7.4), while DCHQ1 was dissolved to a final concentration of 25  $\mu\text{M}$  in DPBS. Different amounts of  $\text{MgSO}_4$  were added and the fluorescence intensities were acquired at 510 nm for DCHQ5 and at 500 nm for DCHQ1. The Mg concentration of the unknown samples were obtained by the interpolation of their fluorescence with the standard curve.

The same protocol was also adopted for hASCs to assess the Mg concentration by DCHQ5.

#### 4.8 Limit of detection

The determination of the limit of detection (LOD) was performed using the following protocol: we prepared three different solutions each containing the same and known amount of Mg ions and we did this for three different increasing amounts of the analyte, always with a fixed chemosensor concentration. For each concentration we registered the fluorescence emission spectra, and we calculated the mean value of emission intensity in the maximum of the band (arithmetic mean). We did the same for all the different concentrations of  $\text{Mg}^{2+}$  and the results were plotted as a function of the metal ion concentration. After performing a linear regression of this curve, we calculated the standard deviation  $\sigma_x$  of the lowest concentration according to the following equation:

$$\sigma_x = \sqrt{\frac{\sum_{i=1}^N (x_i - \bar{x})^2}{N - 1}}$$

The concentration value corresponding to an intensity of  $+ 3\sigma_x$  was taken as the LOD of our system. The LOD was performed for both the two probe in the assay buffer (MeOH:MOPS+10% of DPBS for DCHQ5 and DPBS for DCHQ1) and in sonicated cellular samples.

The detection limit for Mg in AAS was established by analysis of >10 blank solutions (LOD  $3\sigma_{SD}$ ); blank value was  $20 \pm 3$  ng/ml, so the detection limit resulted 6 ng/mL

(0.2  $\mu\text{M}$ ). Trace metals standard (MA-M-2/TM: lyophilized mussels) were analyzed every 20 samples and all values measured for reference materials were within certified limits given by the IAEA (International Atomic Energy Agency).

#### **4.9 Flow cytometry**

Flow cytometric measurements were performed on a Bryte HS cytometer (BioRad, UK), equipped with a Xe-Hg lamp, using a filter set with an excitation band centered at 360 nm and two emission bands centered respectively at 500 nm (for the DCHQ derivatives fluorescence) and 600 nm (for the propidium iodide fluorescence). Before the staining, cells were detached with 0.11% trypsin, 0.02% EDTA, washed twice in DPBS and suspended at a final concentration of  $5 \times 10^5$  cells/mL. The cells were incubated for 15 minutes in the dark at 37°C with DCHQ5 5  $\mu\text{M}$  and DCHQ1 25  $\mu\text{M}$  respectively and then analyzed. Each cell sample was counterstained with 5  $\mu\text{g mL}^{-1}$  propidium iodide (PI) to identify dead cells. Fluorescence distributions were recorded using a logarithmic scale. To assess the intracellular trapping of the dyes, the stained samples were washed in DPBS and reassayed by flow cytometry.

#### **4.10 Cell cycle analysis**

Human adipose-derived mesenchymal stem cells were detached with 0.11% trypsin, 0.02% EDTA, washed twice in DPBS and centrifuged. The pellet was suspended in 0.01% nonidet P-40, 10 mg/mL RNase, 0.1% sodium citrate and 50  $\mu\text{g/mL}$  propidium iodide (PI), for 30 min at room temperature in the dark. Propidium iodide fluorescence was analyzed using a Bryte HS flow cytometer (Biorad,UK) equipped with Hg lamp and analyzed with ModFit (Verity Software House, USA) software.

#### **4.11 Gene expression in hASCs**

Total RNA from control or treated cells was extracted at 5-10 days using the RNeasy Mini Kit (QIAGEN) according to the manufacturer's instructions, and quantified using Nanodrop. One  $\mu\text{g}$  of RNA from each sample was reverse-transcribed into cDNA in a 20- $\mu\text{l}$  reaction volume with SuperScript<sup>TM</sup> III reverse transcriptase

(Invitrogen). To assess gene expression of a panel of markers, 2  $\mu$ l of cDNA were used for real-time PCR performed with a Lightcycler system (Roche Applied Science) and with the GoTaq® qPCR Master Mix (Promega), following the manufacturer's instructions for Fast Cycling Program.

Primers used (0.25  $\mu$ M) were as follows:

GAPDH: forward 5'-CAGCCTCAAGATCATCAGCA-3' and reverse 5'-TGTGGTCATGAGTCCTTCCA-3';

GATA-4: forward 5'-ACCACAGCACAGCCTCATC-3' and reverse 5'-CAGAGCGGGAAGAGGGATTT-3';

HGF: forward 5'-ATTTGGCCATGAATTTGACCT-3' and reverse 5'-ACTCCAGGGCTGACATTTGAT-3';

KDR: forward 5'-CTGCAAATTTGGAAACCTGTC-3' and reverse 5'-GAGCTCTGGCTACTGGTGATG-3';

NANOG: forward 5'-CCTTCCTCCATGGATCTGCTT-3' and reverse 5'-CTTGACCGGGACCTTGTCTTC-3';

NEUROG: forward 5'-CCGCCTTGAGACCTGCATC-3' and reverse 5'-GGCTGCCTGTTGGAGTCTG-3';

NKX-2.5: forward 5'-GCACCCACCCGTATTTATGT-3' and reverse 5'-GGGTCAACGCACTCTCTTTAA-3'.

Data were normalized using GAPDH as an index of cDNA content after reverse transcription. Samples were run in duplicate, and the average threshold cycle (Ct) value was used for calculations. Relative quantification of mRNA expression was calculated with the comparative Ct method using the "delta-delta method" for comparing relative expression results between treatments in real-time PCR [129].

#### **4.12 Fluorescence lifetime imaging (FLIM)**

For the fluorescence lifetime imaging measurements, LoVo S cells were seeded in a glass dish at the concentration of  $1 \times 10^5$  cells/cm<sup>3</sup> for 24h.

Before the analyses, cells were washed twice with DPBS without Ca<sup>2+</sup> and Mg<sup>2+</sup> and directly incubate in the dish with DCHQ5 5 $\mu$ M in the dark for 15 minutes.

The Fluorescence Lifetime Imaging Microscopy (FLIM) experiments were done using a wide field microscope (Leica DM R) in epifluorescence configuration, coupled to a fast gated ICCD camera. The excitation light was provided by a supercontinuum laser source based on a photonics crystal fibre (SuperK EXTREME - NKT photonics, Denmark). The laser is made by two Ytterbium (Yb) doped optical fibres, in the master oscillator/power amplifier configuration, which emits 10 ps pulses at 1080 nm, with a repetition rate selectable from 10 to 40 MHz. The laser light is then processed by a photonics crystal fiber that transforms the narrowband Yb radiation, through non-linear effects, into white light pulses extending from 400 nm to 2400 nm. For the FLIM experiments the repetition rate was set to 20 MHz and an acousto-optic modulator was used to select a 10 nm wide portion of the white spectrum centred around 485 nm. The laser light was then coupled to a large core optical fibre (400  $\mu\text{m}$ ), whose distal end was imaged through a homemade optical system into the focal plane of the microscope, in such a way that the same region of the field of view (about 2/3 of the diameter) was uniformly illuminated using whatsoever objective. The discrimination of the fluorescence emission from the laser light was achieved through a dichroic mirror at 505 nm and a high pass emission filter, with a cut-on wavelength of 500 nm, was employed to remove the residual excitation light.

The detection system was based on a fast light intensifier that can be gated from 200 ps to 1 ns, synchronously with the laser pulses. The intensifier is coupled to a low-noise, cooled CCD camera by means of a high-aperture lens (Picostar, LaVision GmbH, Göttingen, Germany). The light intensifier is synchronised with the laser pulses by a trigger unit made by a fast photodiode coupled to a constant-fraction discriminator and by a jitter free delay generator capable of delays from 0 to 22 ns in 25-ps steps. The jitter of the overall system has been estimated to be less than 50 ps. The whole apparatus is computer controlled by means of software that automatically sets the acquisition parameters (delay, gain of the light intensifier, etc.) and takes the sequence of the gated images.

For the selection of the field of view a 10X objective was used, while all the fluorescence measurements were done with a 63X, 0.9 NA water immersion objective (Leica HCX APO). The optical power in the image plane was 300  $\mu\text{W}$ ,

corresponding to a power density of about 15 mW/cm<sup>2</sup>, with the 63X objective. The gate width of the light intensifier was set to 1 ns and, for each field of view, a sequence of images was acquired with delays of 0, 1, 2, 3, 4, 5, 7, 9, 11, 13, 15, 20 nanoseconds, with respect to the excitation pulses.

The data analysis was done using a custom written software based on the Matlab engine. In each image set, an Area Of Interest (AOI) was selected by visual inspection in order to isolate a discrete number of cells (usually from 1 to 3). Then, the dataset made by the AOIs of all the gated images was processed using a parallel fitting algorithm working, pixel by pixel, with a modified bi- exponential model function.

$$F(d) = A_1 \exp(-d/\tau_1) [1 - \exp(-Gate/\tau_1)] + A_2 \exp(-d/\tau_2) [1 - \exp(-Gate/\tau_2)] + Offset$$

F is the fluorescence, i.e. the integral of the fluorescence intensity within the gate time, d is the acquisition delay for each image of the sequence, A<sub>1</sub>, A<sub>2</sub>, τ<sub>1</sub> and τ<sub>2</sub> are the amplitude and lifetime of the two fluorescence components, respectively, the Offset has been introduced to account for any background noise and the terms [1 - exp (-Gate/τ)] are required to correct for the finite width of the sampling window. The fitting method is based on a standard least mean square algorithm, with initial conditions randomly varied within proper intervals to avoid the convergence of the algorithm toward local minima.

Finally the maps of the parameters A<sub>1</sub>, A<sub>2</sub>, τ<sub>1</sub> and τ<sub>2</sub> are plotted in false colours with a uniform colorbar.

## PART II

### 4.13 Cell culture and reagents

For the comparative analyses of intracellular magnesium in single cells and in a large cell population by atomic force microscopy and X-ray measurements vs DCHQ5, three cellular models (human colon carcinoma cells (LoVo), human endothelial cells isolated from the umbilical vein (HUVEC) and human bone osteosarcoma cells (SaOS2)) were adopted, and variously treated to obtain samples with differences in total Mg content.

Below, are reported the specific protocols adopted for each cell line.

Human colon carcinoma cells LoVo, sensitive (LoVo-S) and resistant (LoVo-R) to doxorubicin were cultured in RPMI 1640, supplemented with 10% FBS, 2 mM glutamine, 100 units/mL penicillin, and 100 µg/mL streptomycin sulfate. To keep the cells resistance to doxorubicin, LoVo-R cell line were fed once every 2 weeks with 1 µg/mL doxorubicin.

Cells were seeded at the concentration of  $1 \times 10^4$  cell/cm<sup>2</sup> and incubated at 37 °C in 5% CO<sub>2</sub> for 24 h before the analyses.

HUVEC were isolated from the umbilical vein and cultured in M199 containing 10% FBS, 1 mM glutamine, 1000 units/mL penicillin and 1 mg/mL streptomycin, endothelial cell growth factor (ECGF) 150 µg/mL, 1 mM sodium pyruvate and heparin (5 units/mL). To evaluate the effect of TRPM7 silencing on magnesium content, a Tet on/Tet off system was used to silence TRPM7 (sample were named +Doxy) after the exposure of the cells to Doxycycline (2ug/ml) for 48h.

To synchronize SaOS2 cells and reduce intracellular magnesium, the cells were cultured for 24h in Mg-free MEM medium with 0.5 % of dialysed FBS. After 24h of Mg and serum deprivation, the cells were switched to a 5% FBS Mg free medium in the presence and absence of MgCl<sub>2</sub> 1 mM for 24h and then analyzed (the samples were respectively named +Mg and -Mg).

For atomic force microscopy and X-ray measurements, all cells lines were plated at a concentration of  $1 \times 10^4$  cell/cm<sup>2</sup> on  $1 \times 1$  mm<sup>2</sup>, 200-nm-thick silicon nitride

(Si<sub>3</sub>N<sub>4</sub>) membrane windows, mounted on a 5 × 5 mm<sup>2</sup> Si frame (Silson) previously sterilized in ethanol. All cell line were treated as reported above, and at the specific times of analyses cells were rinsed with 100 mM ammonium acetate and cryofixed by plunge freezing in liquid ethane and then dehydrated in vacuum at low temperature overnight.

#### **4.14 Quantification of total cell magnesium by DCHQ5**

Total magnesium content was assessed on sonicated cell samples by using the fluorescent chemosensor DCHQ5 as reported in paragraph 4.7.

The Mg concentrations of the unknown samples obtained by the interpolation of their fluorescence with the standard curve were normalized to the cell volume measured as described below in the paragraph 4.15.

#### **4.15 Determination of the cell volume**

All cells lines were detached by trypsinization, centrifuged and resuspended in DPBS at a final concentration ranging between 4000 cells/mL and 8000 cells/mL.

Cells volumes were then calculated counting the cells on a double-threshold Z1 Coulter Counter (Beckman Coulter, USA) and the thresholds were set to cover the interval from 268 to 5575 fL, each step corresponding to an increase of 1 μm in cell diameter. The mean cellular volume was estimated from the Gaussian distribution of the data. The analysis were carried out in triplicate.

#### **4.16 Fluorescence and Scanning Transmission X-Ray Microscopy analysis**

The X-Ray Fluorescence Microscopy (XRFM) and Scanning Transmission X-Ray Microscopy (STXM) measurements were carried out at the beamline Twinmic at Elettra Synchrotron (Trieste, Italy). A Fresnel zone plate focused the incoming beam (1475 eV), monochromatized by a plane grating monochromator, to a circular spot of about 600 nm in diameter. The sample was transversally scanned in the zone plate focus, in steps of 500 nm. At each step, the fluorescence radiation intensity was measured by eight Si-drift detectors (active area 30 mm<sup>2</sup>) concentrically mounted

at a 20° grazing angle with respect to the specimen plane, at a detector-to-specimen distance of 28 mm. Simultaneously, the transmitted intensity T was measured by a fast-readout electron-multiplying low-noise charge-coupled device (CCD) detector through an X-ray–visible light converting system. Zone plate, sample, and detectors were in vacuum, thus avoiding any absorption and scattering by air.

### ***Acquisition Protocol***

Dehydrated cells mounted on the Si<sub>3</sub>N<sub>4</sub> membrane windows were carefully examined with optical microscope and selected following these criteria: integrity, dimensions (large cells require longer acquisition time), and distance from other cells (clustered cells have been avoided because AFM measurements require some free space around the cells). AFM measurements were performed on selected cells before XRFM and STXM measurements. Five STXM images were acquired on whole cells with a step size of 500 nm. In sequence XRFM, and simultaneously STXM, were carried out with a range of 6–8 s dwell time per pixel depending on the cell size. The total acquisition time was in the range of 5–8 h (field of view of at least 20 × 20 μm; spatial resolution 500 nm).

### ***Mass Fraction and Concentration Calculation***

To obtain quantitative information from the measurement of XRFM, we used the fundamental parameter method.

The mass fraction maps  $(w_p)_i$  of each elements were calculated by the following expression:

$$(w_p)_i = \frac{(R_p)_i}{\rho_p \cdot V_p \times Y(E_{0,i}) \times F_p}$$

where  $V_p$  is the volume of the pixel p, expressed in cm<sup>3</sup>, and  $F_p$  is the correction factor for the self absorption of both the incident beam and the fluorescence radiation.

Analogously, the concentration  $(M_p)_i$ , expressed in molarity, is derived by the following expression:

$$(M_p)_i = w_i \cdot \frac{1}{A_i} \cdot \frac{m}{V} \cdot 10^3$$

where  $m$  is the mass expressed in grams, and  $A_i$  is the atomic weight of the element and  $V$  is the volume.

### **Statistical Analysis**

Differences of each experimental condition were evaluated by Student's t test and set as following: \*p<0.05, \*\*p<0.01, \*\*\*p<0.001.

## 5 RESULTS AND DISCUSSION

### *PART I*

#### **5.1 Study of the analytical capabilities of DCHQ5 for the quantitative assessment of total intracellular Mg content**

The first part of this study was focused on the analytical properties of the fluorescent chemosensor DCHQ5 for the quantitative assessment of the intracellular total magnesium content, and its biological applications.

##### **5.1.1 Photophysical Properties of DCHQ5**

We compared the analytical performance of DCHQ5 with the mother probe of the DCHQ family (DCHQ1), which so far was the only dye capable to quantitatively assess intracellular total Mg content [120].

As reported, DCHQ5 shows a significant increase in fluorescence intensity in the presence of Mg ions in MEOH:MOPS solution buffer, while it is not soluble in aqueous buffer, such as Dulbecco's Phosphate Buffered saline (DPBS). On the contrary, DCHQ1 is also soluble in DPBS.

Therefore, a more suitable comparison required the evaluation of the titration profiles of the two chemosensors in the presence of increasing amounts of Mg<sup>2+</sup> in MEOH:MOPS. The titration profile of DCHQ1 was also evaluated in DPBS (Fig. 5.1). Due to the different luminescence quantum yields of the Mg complexes formed with the two dyes, the comparison was performed using concentrations of 25 μM for DCHQ1 and 10 μM for DCHQ5.

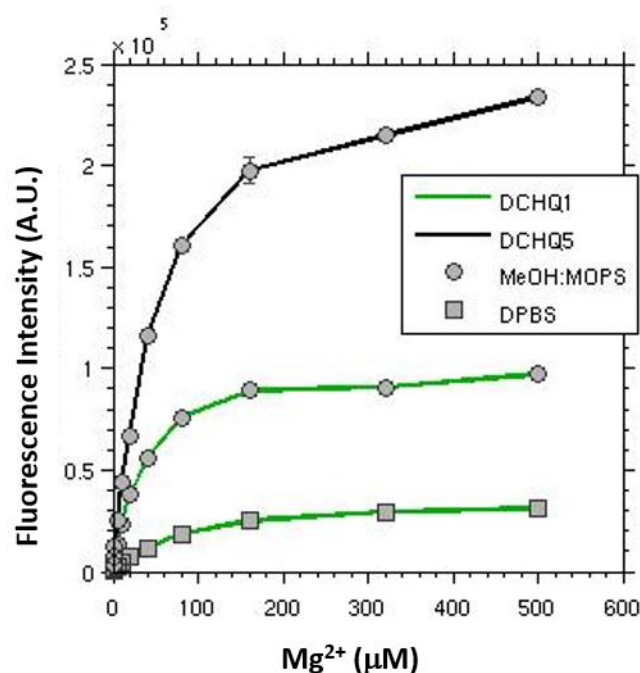


**Figure 5.1:** Fluorescence titration of DCHQ1 (green line, grey dots) and DCHQ5 (black line, grey dots) with  $Mg^{2+}$  respectively at 500 and 510 nm in MeOH:MOPS. The fluorescence intensities are reported normalized for the concentration of the respective probe (25  $\mu M$  for DCHQ1 and 10  $\mu M$  for DCHQ5). Titration of DCHQ1 in DPBS (green line, grey squares) is also reported for comparison.

Fig. 5.1 shows that DCHQ5 has a higher response (represented by the steeper slope) and a higher fluorescence intensity than DCHQ1 for all the Mg concentrations tested. It is also to be noted that the fluorescence intensities were normalized by the respective concentration of the two probes (25  $\mu M$  for DCHQ1 and 10  $\mu M$  for DCHQ5) as indication that the better performance of DCHQ5 was obtained even when using much lower amount than DCHQ1.

All chemosensors are subject to photobleaching to a variable extent, depending on their intrinsic photostability and on the illumination parameters [130]. Since photobleaching causes a decrease in signal strength in proportion to the time and intensity of excitation [131], we assessed the fluorescence stability over time in presence of saturating (Mg:dye ratio of 100:1) and not saturating (Mg:dye ratio of 1:2) concentration of magnesium.

In Table 5.1 are reported the percentage of fluorescence attenuation after 30 minutes of continuous exposure to the excitation light for the two dyes in MeOH:MOPS and also in DPBS for DCHQ1.

**Table 5.1.** Percentage decrements of fluorescence intensity of the two probes at 500 nm for DCHQ1 and at 510 nm for DCHQ5, after 30 minutes of continuous exposure to the excitation light ( $\lambda_{exc}= 360$  nm).

Mg:dye	1:2	100:1
DCHQ1 in MeOH:MOPS	19%	4%
DCHQ1 in DPBS	44%	2%
DCHQ5 in MeOH:MOPS	15%	8%

Results shown that the response of the two dyes in MeOH:MOPS is similar, with a maximum signal decrease in presence of not saturating Mg concentration.

We have also performed the stability test of DCHQ1 in DPBS, because for that probe it is reported a protocol for the assessment of the intracellular Mg content in DPBS [120]. Under these conditions, we observed a marked decrease of fluorescence intensity at the Mg:dye ratio of 1:2, used in the previously proposed intracellular Mg assay protocol.

### **5.1.2 Design of a new protocol for the quantitative assessment of total intracellular magnesium**

Despite the remarkable performances of DCHQ5 in MeOH-based buffer, the perspective to perform assays in cells it is necessarily linked to the use of physiological buffer.

Therefore, we decided to design a new protocol to quantitatively assess intracellular total magnesium in sonicated cellular samples by using a simple spectrofluorimetric assay, based on a standard titration curve.

In particular, DCHQ1 was dissolved in DPBS while DCHQ5 in MeOH:MOPS added with 10% of DPBS, which is the buffer of the sonicated cellular samples.

The addition of that amount of the physiological buffer did not interfere with the fluorescence response of DCHQ5. Indeed, also in the presence of DPBS, the fluorescence intensity of the phenyl derivative remain higher than DCHQ1, and for these assays the concentration used for DCHQ5 was 15  $\mu\text{M}$ , against 25  $\mu\text{M}$  used for DCHQ1.

The fluorescence intensities of known amounts of  $\text{MgSO}_4$  registered for the standard curves were used to determine the Mg concentration of the unknown sonicated cellular samples suspended in DPBS by the interpolation of their fluorescence with the relative standard curve.

We compared the data obtained using DCHQ5 and DCHQ1 in a total of 24 cell samples with various magnesium content, with the ones given by AAS, which is currently the reference technique for the quantification of total intracellular magnesium (Fig. 5.2).

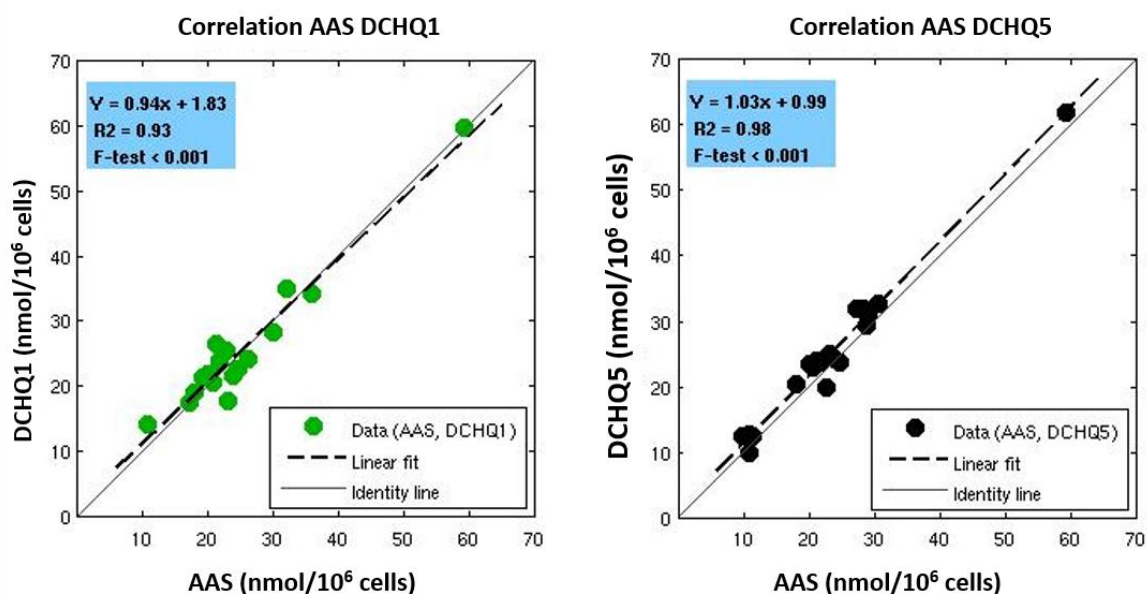


**Figure 5.2.** Correlation between the total intracellular magnesium assessed by AAS and DCHQ1 (on the left) or DCHQ5 (on the right). The identity line is plotted for comparison.

Results show that the values of Mg concentration assessed by both probes overlap the AAS measurements.

Statistical analysis showed that the data could be well fitted with linear equations and we also found a good correlation between the data sets given by the two techniques for both probes, with an R-squared of 0.93 for DCH1 and 0.98 for DCHQ5. We also performed a paired t-test between the dye fluorimetric assays and AAS. Results shown no significance for DCHQ1, while DCHQ5 showed a  $p < 0.01$ . The regression line equation of DCHQ5 has coefficients closer to the identity line than those of DCHQ1. However, the paired t-test analysis showed that DCHQ5 displays a positive systematic deviation from AAS measurements, as can be also noted by the comparison of the correlation with the identity line.

It is worth noting that DCHQ5 can quantitatively assess intracellular total magnesium in much slower number of cells (of the order of  $30\text{-}50 \times 10^3$  cells/mL) compared to DCHQ1, where the minimum cells size per mL is  $100 \times 10^3$ .

To establish the analytical sensitivity of our spectrofluorimetric assay, we then evaluated the Limit of Detection (LOD) for both probes in the assay buffer (MeOH:MOPS +10% of DPBS for DCHQ5 and DPBS for DCHQ1) and also after the addition of the sonicated cellular samples (Table 5.2).

As it is reported in the Table 5.2, for cell populations of  $250 \times 10^3$  and  $100 \times 10^3$  the LOD of the two probes is the same.

As mentioned above, the minimum amount of cells detected by DCHQ1 is  $100 \times 10^3$  cells per mL, while DCHQ5 can quantify Mg even in smaller samples; therefore for DCHQ5 it was possible to establish also the LOD for cellular samples of  $50 \times 10^3$ .

**Table 5.2.** Limit of detection (LOD) of DCHQ1 and DCHQ5 reported in  $\mu\text{M}$  evaluated in the buffer solution (DPBS for DCHQ1 and MeOH:MOPS +10% of DPBS for DCHQ5) and after the addition of cells sample.

Mg <sup>2+</sup> LOD in $\mu\text{M}$ in buffer solution		Mg <sup>2+</sup> LOD in $\mu\text{M}$ sample size (cells/mL)		
		$50 \times 10^3$	$100 \times 10^3$	$250 \times 10^3$
DCHQ1	0.3	n.d	0.2	0.5
DCHQ5	0.2	0.2	0.2	0.5

In parallel, we have also assessed the detection limit in AAS (0.2  $\mu\text{M}$ ) (see paragraph 4.8) and interestingly the LOD of the AAS, a technique generally considered as the gold standard, is of the same order of the LOD measured for DCHQ5 at the lowest sample size, as a proof of the great analytical value of our simple spectrofluorimetric procedure.

### 5.1.3 Cytofluorimetric assays in viable cells

Sonication of samples is a necessary step to quantitatively assess the total cell magnesium by fluorescence spectroscopy, because intracellular membranes and/or lipophilic environments enhanced the fluorescence of the probes [120]. Indeed, it is possible to discriminate substantial changes in total cell magnesium contents by semi-quantitative analysis in viable cells loaded with our dyes in DPBS [114].

In this context, one of the most important limitations of DCHQ1 is its poor intracellular retention. On the contrary, DCHQ5 is highly retained inside the cells. Therefore, we performed cytofluorimetric assays to compare the intracellular retention of the two probes after washing, as well as their fluorescence stability over time inside the cells.

In Fig. 5.3 are reported the mean channel of DCHQs fluorescence of the viable cells in the aforementioned conditions.

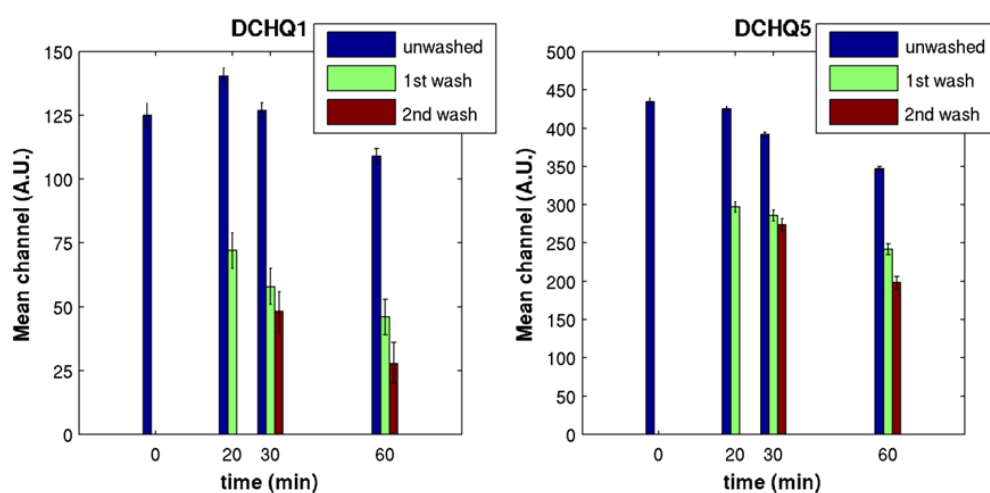


**Figure 5.3:** Mean channel of fluorescence distribution of cells stained with DCHQ1 (on the left) and DCHQ5 (on the right). The measurements were also exploited after the first and the second washing to evaluate the intracellular retention. Data were acquired over a time lapse of 60 minutes after staining. Experiments repeated three times. Data are expressed as mean $\pm$ SD.

As regard the fluorescence stability over time, data shown that the staining is stable up to 60 minutes for both probe, with just a maximum decrease of 20% for DCHQ5. The fluorescence decay can be ascribed to the suffering of cells induced by the capability of DCHQ5 to compete with ATP in binding  $Mg^{2+}$ . Indeed, the micromolar  $K_a(Mg^{2+})$  of the dye is of the same order of magnitude as ATP.

Differences between DCHQ1 and DCHQ5 were more relevant when we considered the intracellular retention evaluated by the mean channel of fluorescence distribution after washing. Data showed that DCHQ5 was much more efficiently retained inside the cells than DCHQ1.

Indeed, the overall fluorescence decrease of DCHQ5 is around the 30% of the initial value, with an almost negligible drop after the second washing. Conversely, DCHQ1 fluorescence progressively decrease after the second washing, with a total decrement of 80% from the initial value. These results suggest that for DCHQ5 the first washing eliminates only the dyes loosely bound to the cellular surface, and not the probe entrapped within the cell, which unlike DCHQ1, is not removed by the second washing.

Another important aspect that has to be considered is the concentration of the dyes used allowing the best compromise between high signal and low cytotoxicity. For the cytofluorimetric assays the amount of DCHQ5 required is one fifth ( $5\ \mu\text{M}$ ) than that for DCHQ1 ( $25\ \mu\text{M}$ ), a further evidence of the great analytical value of DCHQ5 also in live cells analysis.

## 5.2 Fluorescence Lifetime Imaging of DCHQ5

A common characteristic of the members of the DCHQ family is to show a bi-exponential fluorescence lifetime decay in the intracellular environment. In particular, for the mother probe DCHQ1 are reported two fluorescence lifetime by using Time-Correlated Single Photon Counting (TCSPC) in cell suspensions of HC11 and HL60 cells [115]. However, for DCHQ1 the excitation is possible only in the UV region, where the background interference due to cell auto-fluorescence, notably limit its application in fluorescence lifetime imaging (FLIM) microscopy.

FLIM has been recognized as a powerful microscopy technique that can map the spatial distribution of the fluorescence lifetime of a fluorophore in a single cell providing quantitative information on intracellular environments. Furthermore, this technique is independent of fluorophore concentration, fluorescence intensity, light path length and photobleaching [132].

Among the members of the DCHQ family, DCHQ5 possesses the unique feature to be excitable in the visible region. This property renders this dye very interesting for fluorescence lifetime imaging (FLIM) applications, since in the visible region the background interference is minimized.

Therefore, we also performed FLIM measurements in collaboration with the group of Professor Paola Taroni at the Politecnico of Milan to explore the capability of DCHQ5 to obtain FLIM image of intracellular Mg.

In Fig 5.4 are reported the data obtained in a typical experiment in LoVo cells, were are depicted the intracellular distribution maps of T1 and T2 and of the amplitude A1 and A2, which represent the complex Mg:dye (see equation in paragraph 4.12).

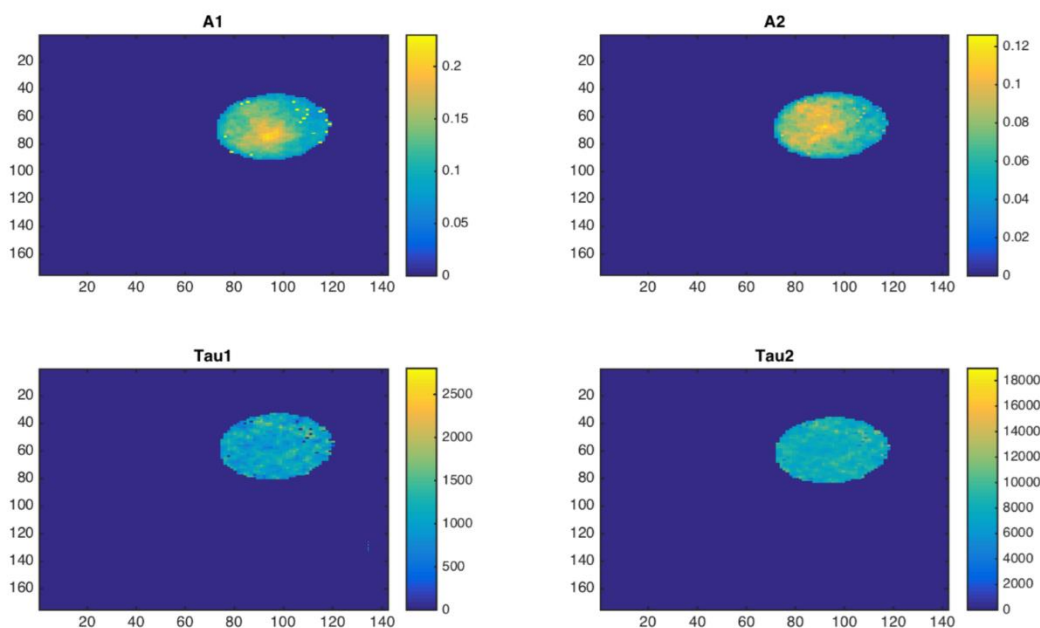


**Figure 5.4:** Intracellular distribution maps of the two lifetimes decay T1 and T2 and of the corresponding A1 and A2 in a typical LoVo cell loaded with DCHQ5 5 $\mu$ M in DPBS.

Results displayed a homogeneous distribution of T 1 and T 2 inside the cell, while we observed different pattern of distribution of A1 and A2, which is an extremely interesting data, since the amplitudes represent the patterns of distribution of the complex Mg:dye inside the cells.

Indeed, FLIM image of intracellular Mg has never been done so far, and in light of these achievements, now we can further understand and explain previously reported results of our group about the intracellular distribution of magnesium by two-photon confocal imaging [114].

As it is shown in the Fig.5.5, taken from Marraccini et al, cells loaded with DCHQ5 disclosed a diffused fluorescence over the cytosol with a higher intensity in the perinuclear region. Moreover, DCHQ5 presented a high fluorescence signal also in the plasma cell membrane, accordingly with the fluorescence enhancement of DCHQs derivatives in the lipophilic environment [120].

Matching together the results of the two imaging technique, we can deduce that the higher fluorescence of DCHQ5 previously observed by our group in the cell membranes by two-photon microscopy was related to a higher concentration of

magnesium in these environments and not to the effect of a heterogeneous distribution of the two lifetimes within the cell, as we have proved.

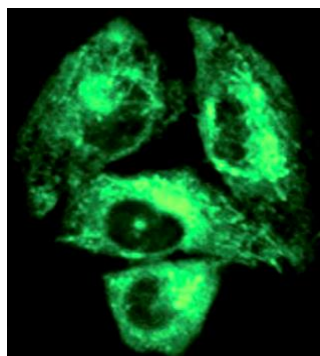


**Figure 5.5:** Two photon fluorescence microscopy image ( $\lambda_{exc}=750$  nm), of ROS rat osteosarcoma cells stained with DCHQ5 10 $\mu$ M. (Panel D taken from the Fig. 6 of Marraccini et al. 2012 [114]).

In particular, the higher fluorescence intensity found in the perinuclear region, corroborates the evidence that in this area there is a physiological accumulation of magnesium due to the presence of several sub-cellular organelles [109], [133].

Also in the plasma membrane, DCHQ5 showed a high fluorescence signal intensity which, according to our results, would correspond to a high concentration of Mg<sup>2+</sup>. This interpretation is supported by the “Membrane Magnesium Mitosis” model of cell proliferation control postulated by Rubin [81]. According to this theory, the pool of magnesium bound to the inner surface of the plasma membrane plays a crucial role in the regulation of cell proliferation. Indeed, membrane perturbations, induced by the binding of growth factors to their receptors, provoke the release of membrane bound magnesium, which triggers the proliferating signaling to the nucleus.

### **5.3 Study of the magnesium involvement in the commitment of human adipose-derived mesenchymal stem cells**

The real contribution of magnesium to the complex and articulate process of cell differentiation is not clear and data reported in literature are few and discordant. Among the field of cell differentiation, in the last decades, growing interest have been arising to the application of human mesenchymal stem cells (hMSCs) for regenerative medicine [56]. Indeed hMSCs are able to self-renew and possess multipotent differentiation properties. In particular, adipose tissue has been identified as an abundant and easily accessible source of multipotent adipose-derived stem cells (hASCs) [134]. Furthermore, it has been reported that the treatment of hMSCs with a mixture of differentiating agents, such as hyaluronic, butyric and retinoic acids, remarkably increased the multipotent commitment of these cells [56]–[58].

#### **5.3.1 Total magnesium content and cell cycle analyses of hASCs in complete and Mg-free medium**

Based on the findings mentioned above, we decided to investigate the role of magnesium in the preconditioning of human adipose-derived mesenchymal stem cells (hASCs) with a mixture of hyaluronic, butyric and retinoic (HBR) acids.

In Fig. 5.6, panel A, are reported the total Mg concentrations of treated (HBR) and untreated (Ctr) hASCs cells in complete medium at 0, 2, 5 and 10 days of analysis. The treatment with the cocktail of differentiating agents was carried out at time 0. The measurements were performed in sonicated sample by using the fluorescent probe DCHQ5 as reported in paragraph 4.7.

In parallel we have also evaluated the cell cycle distribution by flow cytometry (Panel B).

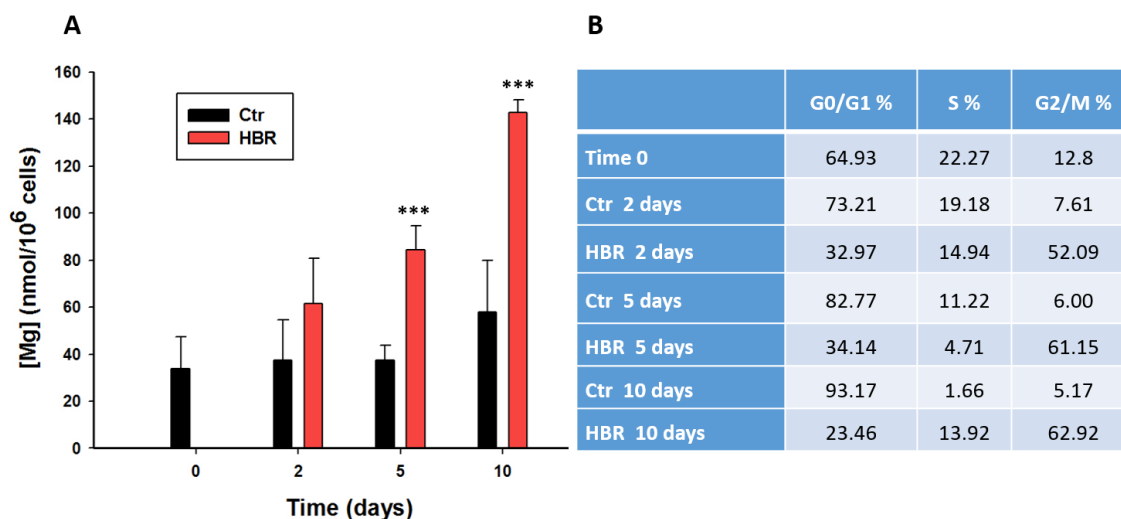


**Figure 5.6:** Panel A: Total Mg concentration of treated (HBR, red bar) and untreated (Ctr, black bar) hASCs cells at 0, 2, 5 and 10 days of analysis in complete medium. Measurement were carried out in sonicated sample by using the fluorescent probe DCHQ5

\*\*\* Significantly different from the control,  $p < 0.001$ . Panel B: Cell cycle distribution in hASCs treated and untreated at the same times.

Interestingly, the total magnesium quantification by DCHQ5 revealed a surprising and progressive increment of magnesium in treated cells from day 2 to 10 compared to control cells. In particular, at time 5 and 10 days the increase in cells treated with HBR is statistically significant. As shown in Fig. 5.6, panel A, total intracellular magnesium content at 5 days in cells preconditioned with HBR is  $84.6 \pm 10.5$  nmol/10<sup>6</sup> cells, two times more than in control cells, which present an average concentration of  $37.6 \pm 6.1$  nmol/10<sup>6</sup> cells. At 10 days, the difference is even more relevant, with an increment in treated cells ( $142.8 \pm 5.4$  nmol/10<sup>6</sup> cells) more than three times higher than the control ( $57.8 \pm 22$  nmol/10<sup>6</sup> cells). Moreover, the increment of magnesium in treated cells is accompanied by a remarkable accumulation in the G2/M phase of the cell cycle as compared to the untreated samples at all time of analysis (2, 5 and 10 days), as shown in Panel B.

It is important to highlight that quantification of total intracellular Mg by using DCHQ5 allowed us to accurately assess total magnesium content in very small cellular samples, of the order of  $25\text{-}30 \times 10^3$  cells/mL. Taking into account the

relatively small number of cells that we had for these analyses, these measurements could not be carried out by other available techniques, as AAS, that requires a more consistent amount of cells, at least  $1 \times 10^6$ /mL.

Since extracellular  $Mg^{2+}$  availability differently affected cell differentiation depending on the cell model investigated, we have also performed the same experiments in Mg-free medium.

In figure 5.7, panel A, are reported the total Mg concentrations of treated (HBR -Mg) and untreated (Ctr -Mg) hASCs cells in Mg-free medium at 0, 2, 5 and 10 days of analysis.

Also in these set of experiments, the treatment with the cocktail of differentiating agents was carried out at time 0. Again, in parallel we have evaluated the cell cycle distribution by flow cytometry (Panel B).

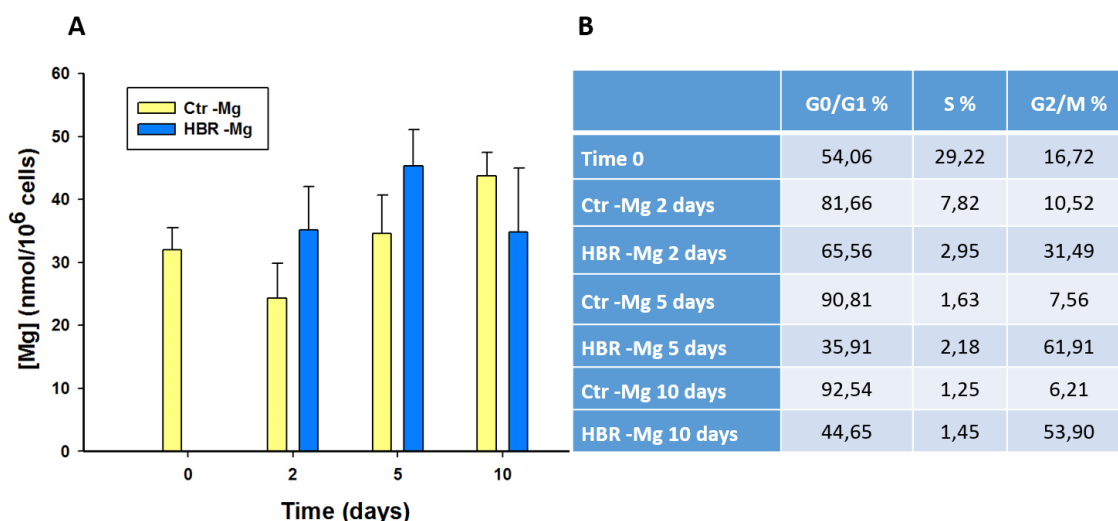


**Figure 5.7:** Panel A: Total Mg concentration of treated (HBR -Mg) and untreated (Ctr -Mg) hASCs cells at 0, 2, 5 and 10 days of analysis in Mg-free medium. Measurement were carried out in sonicated sample by using the fluorescent probe DCHQ5. Panel B: Cell cycle distribution in hASCs treated and untreated at the same times.

As regard the total magnesium content measured by DCHQ5, in Mg-free medium we do not observed significant difference between control and treated cells at any

times, as expected since the cells were kept in a complete Mg-free medium for all the time.

The magnesium fluctuations of both control and treated cells, are to be ascribed to the internal heterogeneity of hASCs and are amplified by the large scaling adopted in the graphic.

Even in this set of experiment, we observed an accumulation in the G2/M phase of the cell cycle as compared to the untreated samples at all time of analysis (2, 5 and 10 days), as shown in Panel B, even if the accumulation in G2/M phase at 2 days is more marked in complete medium than in Mg-free (HBR: G2/M 52.09 %; HBR -Mg: G2/M 31.49%).

Furthermore, in treated and Mg-deprived cells the G1 phase is higher than treated cells in complete medium at all times.

Taken together, these findings prompt to hypothesize that the pre-commitment of hASCs is strictly related to the block of the cell cycle at G2/M phase, since in both complete and Mg-free medium, the accumulation in G2/M took place only when the cells are exposed to the mixture of differentiating agents. However, in treated and Mg-deprived cells the accumulation in G2/M increases over time, while in complete medium it is already at the maximum after two days of treatment. This evidence suggests that magnesium deprivation could delay this accumulation.

This is an unusual results if compared to data reported in literature, since recent studies shown that Pluripotent Stem Cells (PSC) are more prone to respond to differentiation in the G1 phase of the cell cycle, suggesting a correlation between PSC differentiation and G1 phase [135]. Anyway, understanding the mechanisms that govern the processes of self-renewal and lineage specification continues to be a few explored field. Moreover, in literature there are no evidence about the cell-cycle state and pre-commitment of hASCs.

On the other hand, in agreement of our observation, it is reported the induction of cell differentiation in G2/M phase in rat neural cells exposed to apigenin [136] and in Caco-2 cells treated with nocodazole [137].

Moreover, it is also reported that butyric acid is the major effector of cell cycle accumulation in G2/M in a dose dependent manner [138].

As regard the magnesium content of hASCs, taking into account the time dependent increase of total intracellular magnesium of treated cells in complete medium, a correlation between magnesium and cell commitment seems to exist. Indeed, these increase is a counterintuitive results since the knowledge that proliferating cells contain more  $Mg^{2+}$  than resting ones is well established, coherently with the promoting role of  $Mg^{2+}$  on protein and DNA synthesis [101]. Conversely, hASCs are poor proliferating cells with a slow rate of growth, which is further reduced by the treatment with the cocktail of differentiating agent. In fact, the cocktail of differentiating agents stimulated the pre-commitment of hASCs, which is a process that necessarily implicates a metabolic stimulus and reorganization aimed at achieving a terminal commitment. For example, it is reported that HBR increase the expression of a number of gene enrolled in stem cell survival and/or cardiovascular commitment in vitro [139]. Hence, HBR preconditioning of hASCs is far from being a quiescent state.

### **5.3.2 Analyses of gene expression of a panel of multilineage markers in complete and Mg-free medium**

In order to understand whether and how magnesium availability was involved in HBR preconditioning of hASCs, we examined the gene expression of a panel of markers representing the multilineage potential of these cells, such as GATA-4, NKX-2.5, HGF, KDR, NEUROG and NANOG.

GATA-4 (GATA Binding Protein 4) and NKX-2.5 (NKX2 Homeobox 5) are two key regulators of cardiogenic commitment, in particular, the latter is the earlier known marker of the cardiac lineage [140], [141], HGF (Hepatocyte Growth Factor) and KDR (Kinase Insert Domain Receptor) are involved in the orchestration of vasculogenesis and proper capillary formation [142], [143], NEUROG (Neurogenin) is a marker of neurogenic commitment [144] while NANOG (Nanog Homeobox) is a gene involved in the maintenance of stem cells pluripotency [145].

We evaluated the gene expression at 5 and 10 days for treated and untreated cells both in complete and Mg-free medium.

In Figure 5.8, are depicted the mRNA level of the cardiac lineage-promoting genes GATA-4 (on the left) and NKX-2.5 (on the right).

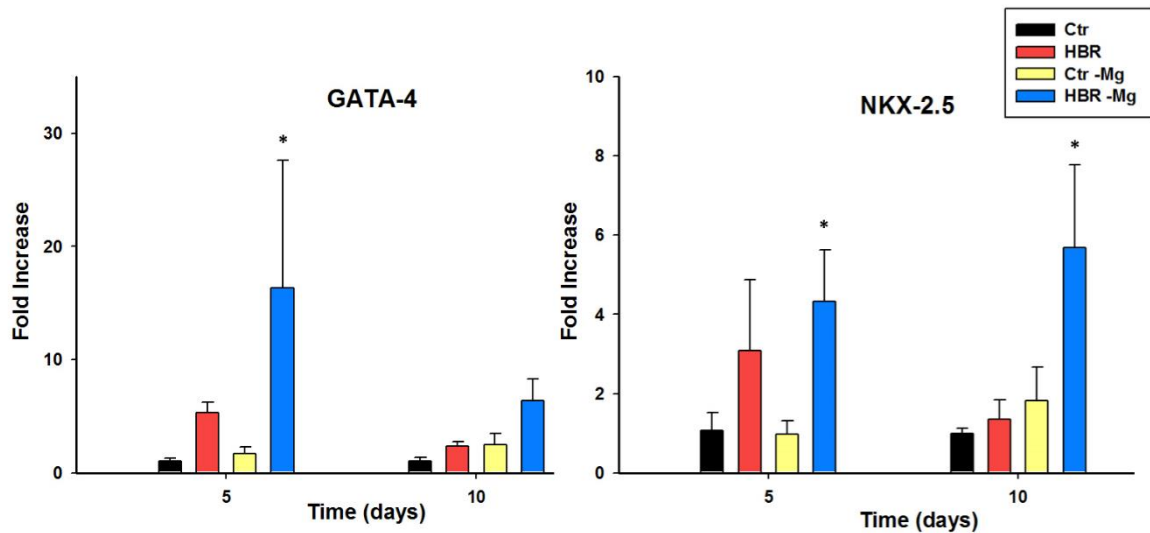


**Figure 5.8:** Analysis at 5 and 10 days of gene expression of the cardiac lineage-promoting genes GATA-4 (on the left) and NKX-2.5 (on the right) in complete medium (control (Ctr) and treated (HBR) cells), and in Mg-free medium (control (Ctr -Mg) and treated (HBR -Mg) cells).

\*Significantly different from the treated samples in complete medium (HBR),  $p < 0.05$ .

Results shown that the gene expression of the two key regulators of cardiogenic commitment is strongly enhanced in cells treated with HBR and grown under Mg-free conditions compared to treated cells in complete medium. In particular the gene expression acceleration is significantly different for GATA-4 only at 5 days, while for NKX-2.5 at both 5 and 10 days.

As regard the gene expression of the vasculogenesis markers HGF and KDR, as shown in Fig. 5.9, we observed the same trend.

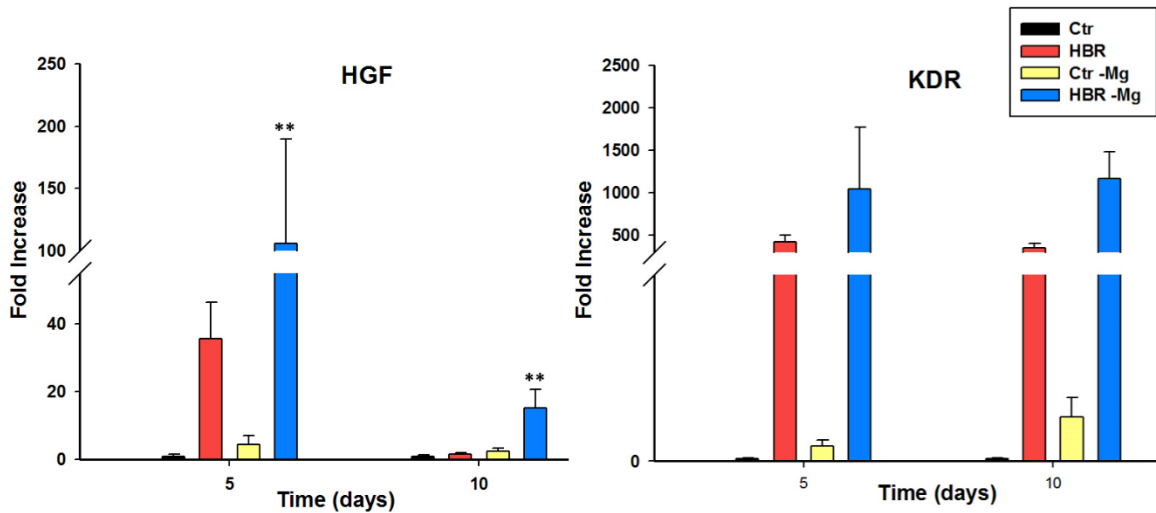


**Figure 5.9:** Analysis at 5 and 10 days of gene expression of vasculogenic genes HGF (on the left) and KDR (on the right) in complete medium (control (Ctr) and treated (HBR) cells), and in Mg-free medium (control (Ctr -Mg) and treated (HBR -Mg) cells). \*\*Significantly different from the treated samples in complete medium (HBR),  $p < 0.01$ .

Indeed, also for this panel of markers, in Mg-free medium the mRNA level of treated cells is further enhanced, with significant differences both at 5 and 10 days for HBR, compared to treated cells in complete medium.

Lastly, as shown in Fig. 5.10, in order to have a complete picture of the possible cells lineages of hASCs, we evaluated the effects of Mg deprivation also in NEUROG, our markers for the neurogenic commitment and NANOG, a gene involved in the maintenance of the pluripotency, to investigate in parallel even the self-renewal potentiality in our system.

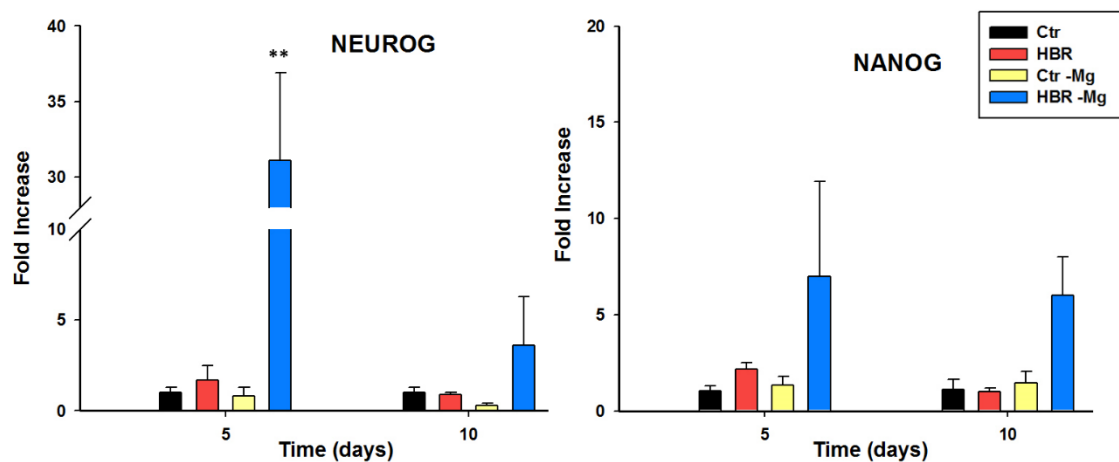


**Figure 5.10:** Analysis at 5 and 10 days of gene expression of neurogenic gene NEUROG (on the left) and of NANOG (on the right), which is a gene involved in the maintenance of the pluripotency, in complete medium (control (Ctr) and treated (HBR) cells), and in Mg-free medium (control (Ctr -Mg) and treated (HBR -Mg) cells). \*\*Significantly different from the treated samples in complete medium (HBR),  $p < 0.01$ .

Also for these markers, we observed the same trend even if the differences are statistically significant only for NEUROG at 5 days.

Taking together the data about the gene expression, they seem to indicate that the effects of the treatment with HBR is strongly accelerated by the magnesium deprivation.

Indeed, in hASCs stimulated by HBR, for all the genes under investigation, we have found an increase of the gene expression in Mg-free medium compared to complete one. Even though this trend was present in each experiment, we had high standard deviation for NEUROG and NANOG at 10 days, for KDR both at 5 and 10 days and for GATA-4 at 10 days, and the mean gene expression reported for these markers did not reach the threshold of significance.

Since the gene expression of the panel of markers that we have investigated is enhanced by the Mg deprivation, to further dissect the involvement of magnesium

in the multilineage modulation of gene expression, we decided to examine the response of these markers after the re-addition of magnesium to the deprived medium.

In particular, we grown the pre-conditioned cells in Mg-free medium for 5 days and then we add again MgCl<sub>2</sub> 1mM to the medium, for other 5 days. Hence, the gene expression was evaluated at the final time of 10 days and we compared treated cells in all condition under analysis: complete medium (HBR, red bar), Mg-free medium (HBR -Mg, blue bar) and Mg-free medium with the re-addition of MgCl<sub>2</sub> at day 5 (HBR Mg re-add, green bar).

In Fig. 5.11 are depicted the results at 10 days of all the markers in the three conditions mentioned above.

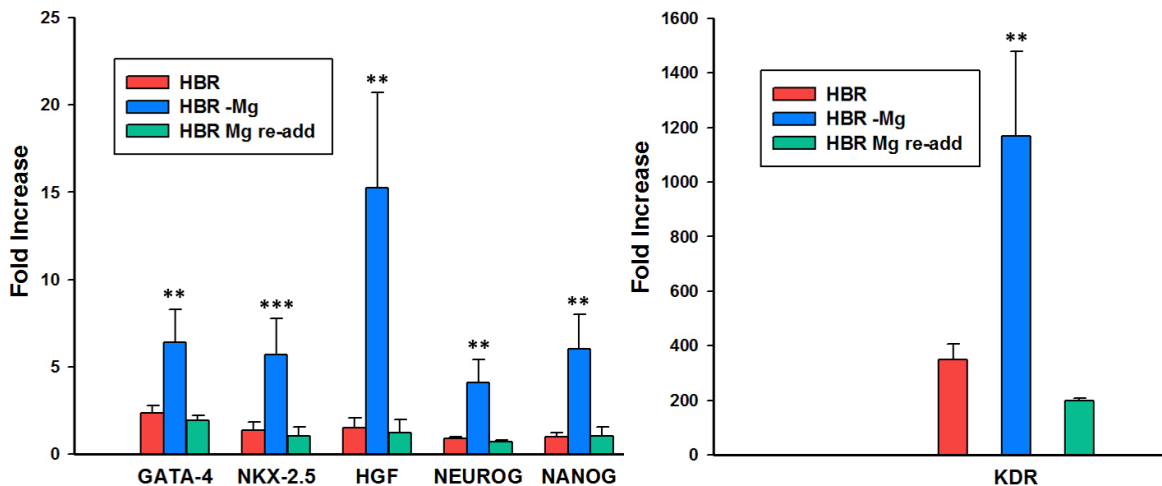


**Figure 5.11:** Analysis at 10 days of gene expression of GATA-4, NKX-2.5, HGF, NEUROG and NANOG (on the left) and of KDR (on the right) of treated cells in complete medium (HBR, red bar), Mg-free medium (HBR -Mg, blue bar) and after 5 days of Mg re-addition to the deprived medium (Mg re-add, green bar). All the values were normalized respect to their controls.

\*\*  $p < 0.01$ , \*\*\*  $p < 0.001$ : significantly different from the treated samples deprived of magnesium and then supplemented with MgCl<sub>2</sub> for 5 days (HBR Mg re-add).

Results shown that the re-addition of magnesium for 5 days to the deprived medium, further modulated gene expression, but in a negative way: in fact the expression of

all the genes decreases to the same level of that obtained in samples grown in complete medium.

Altogether, the results clearly show that the magnesium deprivation trigger the enrichments of the multilineage preconditioning of hASCs exposed to the mixture of differentiating agents, since gene expression of the markers investigated was strongly enhanced only in the cells constantly grown in Mg-free medium.

## *PART II*

Recently, one of the main focus of life science in elemental quantification is direct to single cell analysis. Indeed, the possibility to have a map of whole single cells could give important informations about morphology of the cell, amount of element constituting the cell and more important the elemental distribution and compartmentalization in the cell organelles.

In particular, synchrotron x-ray fluorescence microscopy is a highly sensitive method for mapping elements distribution in single cells at nanoscale resolutions [128].

The knowledge that this kind of techniques can gives about cell biology are extremely significant but the information obtained in small group of single cells should not disregards the behaviour of a large population of cells.

In this context, in the second part of this study we decided to compare single cells analysis performed with synchrotron-based fluorescence and cell population analysis carried out by the fluorescent chemosensor DCHQ5. In particular, we compared the concentration of intracellular Mg obtained with the two methods.

Single cells analyses were performed by adopting a multidisciplinary approach, with the use of complementary techniques and implementation of custom-made algorithms which allowed us to obtain molar concentration maps of  $Mg^{2+}$  and of fundamental life elements, such as carbon (C), nitrogen (N) and oxygen (O) in whole single cell. To do this, we combined Atomic Force Microscopy (AFM), with synchrotron based X-ray fluorescence Microscopy (XRFM) and Scanning Transmission X-ray Microscopy (STXM) in whole dehydrated cells [99].

All the synchrotron-based fluorescence analyses were carried out at Twinmic beam line at the Elettra synchrotron of Trieste.

## 5.4 Synchrotron-based single cells analysis

We have analysed three different cellular models variously treated to obtain differences in the total magnesium content. Endothelial cells isolated from the umbilical vein (HUVEC) were measured in a single experiment where we have analysed five wild type HUVEC (controls) and five HUVEC genetically engineered to silence TRPM7 (TRPM7 silenced) after the expositions of cells to Doxycycline (2 $\mu$ g/ml) for 48 h (Tab1). In the second experiments, we investigated the different distribution and content of intracellular Mg in SaOS2 cells cultured in a medium containing 0.5% FBS in the absence of MgCl<sub>2</sub> to synchronize cells in G<sub>0</sub>/G<sub>1</sub> phase and reduce intracellular Mg content. After 24h of starvations, control cells (+Mg) were kept for other 24 h in a Mg-free medium supplemented with MgCl<sub>2</sub> 1 mM, while the deprived cells (-Mg) were kept for the following 24 h in the Mg- free medium. In total we have analysed four controls and four deprived samples.

Regarding the last cellular model, LoVo cells were acquired in three different experiments where we were interested to study the intracellular concentration and distribution of magnesium in LoVo sensitive (LoVo S) and resistant (LoVo R) to doxorubicin, one of the most used anticancer drug.

This approach allow to obtain physical property such as density, volume and mass in addition to elemental composition such ad concentration.

Table 5.3 (HUVEC and SaOS2), and Table 5.4 (LoVo) shown the molar concentrations of carbon (C), nitrogen (N), oxygen (O), and magnesium (Mg) derived by synchrotron-based single cells analysis in the three cellular.

**Table 5.3:** Whole cell parameters<sup>a</sup> in HUVEC cells, wild type (Controls) and silenced for TRPM7 (TRPM7 silenced) and in SaOS2 cells, cultured in presence (+Mg) and absence (-Mg) of Mg.

SYNCHROTRON (single cell(s) analysis)									
Sample		Fixation	Density	Volume	Mass	Concentration			
HUVEC			g/cm <sup>3</sup>	μm <sup>3</sup>	pg	C (mM)	N (mM)	O (mM)	Mg (mM)
Controls	H6	Cryo	1.79	114	204	69941	23296	19311	109
	H7	Cryo	1.14	125	142	44552	14015	13298	89
	H8	Cryo	1.31	273	358	51512	14057	12089	90
	H9	Cryo	1.62	161	261	61020	19788	16451	111
	H10	Cryo	1.58	107	169	62571	19621	16946	102
Mean			1.49	156	227	57919	18155	15619	100
SD			0.26	69	86	9944	4037	2913	10
CV			17%	44%	38%	17%	22%	19%	10%
TRPM7 silenced	H1	Cryo	1.37	156	214	43202	13242	11156	87
	H2	Cryo	1.44	147	211	57878	20996	17706	164
	H3	Cryo	1.36	209	283	51805	19682	15763	111
	H4	Cryo	1.45	129	187	53719	21419	16429	104
	H5	Cryo	1.4	142	199	56929	24314	17842	58
Mean			1.40	156.60	218.80	52707	19931	15779	105
SD			0.04	30.88	37.45	5847	4104	2728	39
CV			3%	20%	17%	11%	21%	17%	37%
									n.s
Sample		Fixation	Density	Volume	Mass	Concentration			
SaOS2			g/cm <sup>3</sup>	μm <sup>3</sup>	pg	C (mM)	N (mM)	O (mM)	Mg (mM)
+ Mg	S1	Cryo	1.21	110	134	49765	26786	16761	92
	S2	Cryo	1.27	110	140	43537	23730	14017	87
	S3	Cryo	1.32	81	107	50450	23628	16008	102
	S4	Cryo	1.33	111	148	51088	23210	12991	87
Mean			1.28	103	132	48710	24339	14944	92
SD			0.06	15	18	3491	1647	1742	7
CV			4%	14%	13%	7%	7%	12%	8%
- Mg	S5	Cryo	1.30	115	149	51178	26192	15068	45
	S6	Cryo	1.51	211	318	61004	25265	13497	31
	S7	Cryo	1.46	127	185	61353	24955	12974	26
	S8	Cryo	1.40	203	283	57765	22292	14161	31
Mean			1.42	164	234	57825	24676	13925	33
SD			0.09	50	80	4717	1674	904	8
CV			6%	30%	34%	8%	7%	6%	25%
									p<0.05

<sup>a</sup> For each cell, total volume calculated from AFM and total mass and mean density calculated from the respective mass and density maps are reported. The calculated concentration of the elements are also reported for each cell (HUVEC: 4 controls and 4 TRPM7 silenced; SaOS2: 4 +Mg and 4 -Mg). SD, standard deviation; CV, coefficient of variation. For Mg concentration the value of the t-test is also reported.

**Table 5.4:** Whole cell parameters<sup>a</sup> in LoVo cells, sensitive and resistant to doxorubicin

SYNCHROTRON (single cell(s) analysis)									
Sample		Fixation	Density	Volume	Mass	Concentration			
LoVo			g/cm <sup>3</sup>	μm <sup>3</sup>	pg	C (mM)	N (mM)	O (mM)	Mg (mM)
S e n s i t i v e	L1 A	Chem	1.16	174	201	38388	17286	15059	55
	L2 A	Chem	1.09	176	191	44419	17657	14699	42
	L3 A	Chem	1.16	106	123	45222	20465	16568	17
	L4 B	Cryo	1.43	90	129	58026	17511	15823	43
	L5 B	Cryo	1.11	261	289	40718	13725	12964	84
	L6 B	Cryo	1.14	347	397	43020	12602	12203	95
	L7 B	Chem	1.75	144	253	56173	24654	20926	59
	L8 B	Chem	1.81	155	280	48704	25460	25051	72
	L9 C	Cryo	1.11	177	196	42461	18264	15586	73
	L10 C	Cryo	1.13	164	186	43930	17407	14136	24
	L11 C	Cryo	0.95	81	77	36900	13515	12246	51
	L12 C	Cryo	1.22	133	162	46114	19111	14774	95
	L13 C	Cryo	1.09	112	122	46235	17106	14144	45
	L14 C	Cryo	1.24	196	243	51653	18014	15191	102
<b>Mean</b>			<b>1.24</b>	<b>165</b>	<b>204</b>	<b>45855</b>	<b>18056</b>	<b>15669</b>	<b>61</b>
<b>SD</b>			<b>0.25</b>	<b>70</b>	<b>84</b>	<b>6105</b>	<b>3688</b>	<b>3448</b>	<b>27</b>
<b>CV</b>			20%	42%	41%	13%	20%	22%	43%
R e s i s t a n t	L17 B	Cryo	0.97	139	135	36764	14150	13168	83
	L18 B	Cryo	1.18	171	202	40057	16216	14432	87
	L19 B	Chem	1.83	142	261	59311	27845	23832	66
	L20 B	Chem	1.42	192	272	47011	21828	18849	60
	L21 C	Cryo	1.11	78	87	43338	23071	17314	79
	L22 C	Cryo	1.21	73	88	48208	27085	18380	65
	L23 C	Cryo	1.52	157	239	56129	31196	22804	96
	L24 C	Cryo	1.24	65	81	44821	28428	18980	62
	L25 C	Cryo	1.29	89	115	49693	25146	17551	76
	L26 C	Cryo	0.95	44	42	39746	17581	13302	52
	L27 C	Cryo	1.20	83	100	44771	21487	15559	47
<b>Mean</b>			<b>1.27</b>	<b>112</b>	<b>147</b>	<b>46350</b>	<b>23094</b>	<b>17652</b>	<b>70</b>
<b>SD</b>			<b>0.25</b>	<b>49</b>	<b>81</b>	<b>6839</b>	<b>5465</b>	<b>3498</b>	<b>15</b>
<b>CV</b>			20%	44%	55%	15%	24%	20%	22%
<b>n.s</b>									

<sup>a</sup> For each cell, total volume calculated from AFM and total mass and mean density calculated from the respective mass and density maps are reported. The calculated concentration of the elements are also reported for each cell (14 LoVo S and 11 LoVo R). Results of three experiments, indicated as A, B, C. SD, standard deviation; CV, coefficient of variation. For Mg concentration the value of the t-test is also reported.

As is shown in the tables below, this approach allow to obtain physical property such as density, volume and mass in addition to elemental composition, in particular the concentration.

Focusing the attention on the results about Mg content, using single cells analysis, we found a statistically different quantities of Mg in SaOS2 cells ( $p < 0.001$ ), denoting a decreasing of Mg in deprived cells ( $33 \pm 8$  mM), compared to control cells ( $92 \pm 7$  mM).

The main goal of our multidisciplinary approach was the possibility to reconstruct detailed maps of the spatial distribution of cell density and mass by merging STXM information (electron density of the sample) and cell thickness map obtained by AFM aligned onto STXM space, providing the volume of each single cell analysed.

Finally, molar concentration distribution were obtained by normalizing the maps of fluorescence intensity respectively to the volume maps.

This accurate approach provides both submicrometer spatial resolution and quantification of elements down to  $10^6$  atoms/ $\mu\text{m}^3$  (based on the minimum concentration detected in a single pixel for each element, i.e., 1 mM) as shown in Fig. 5.12, for a representative cell.

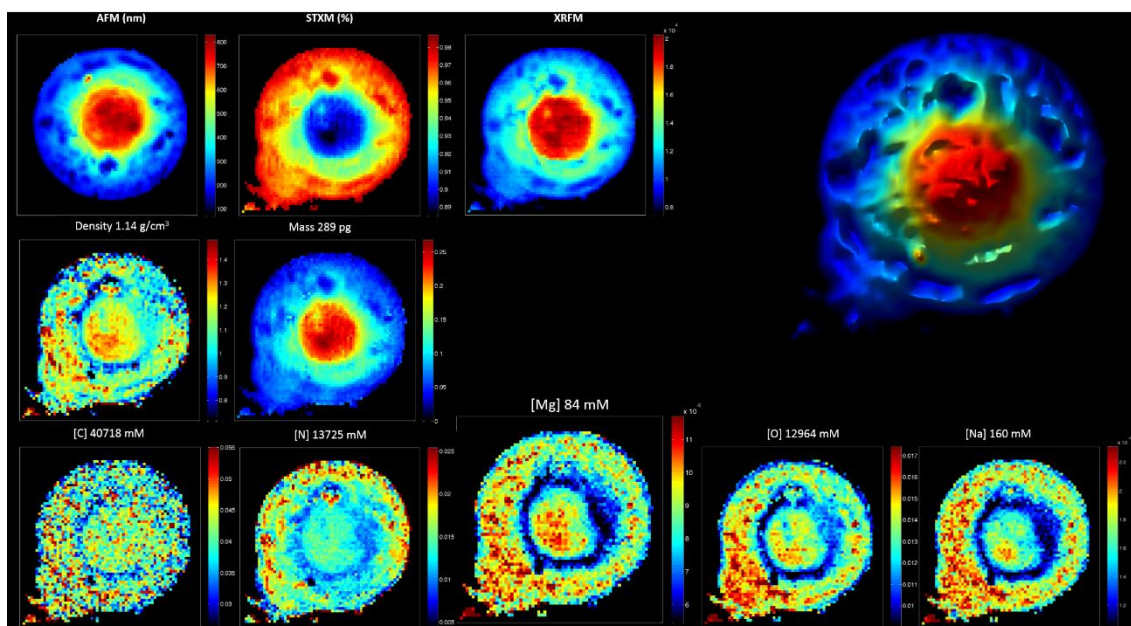


**Figure 5.12:** (Top row, from the left): morphology, X-ray transmission, and X-ray fluorescence images of a LoVo S (cell L5 B reported in TableXXX), acquired by atomic force microscopy (AFM), scanning transmission X-ray microscopy (STXM), and X-ray fluorescence microscopy (XRFM), respectively. The XRFM image reports the sum of all the channels of the spectrum. In the top right panel is shown a 3D rendering of AFM. (Second row): from AFM and STXM is then calculated a map of the spatial distribution of the cell density and mass. (Third row): Elemental maps of molar concentration of C, N, O and Mg.

## 5.5 Cell population analyses by DCHQ5

In parallel to the synchrotron-based fluorescence analyses we quantified the total amount of intracellular Mg in a large population of the same samples by using DCHQ5 (Table 5.5 and Table 5.6).

Moreover, we calculated the exact volume of all the cells type under investigation by using Beckman coulter counter (see Paragraph 4.15), and we normalized the amount of magnesium assessed by spectrofluorimetric assay to the calculated cells volumes, in order to obtain the molar concentration of total intracellular Mg in a large population, as reported in Table 5.5 for HUVEC and SaOS2 cells, and in Table 5.6 in LoVo cells.

**Table 5.5.** Molar concentration of Mg assessed by DCHQ5 in HUVEC (controls and TRPM7 silenced) and SaOS2 (+Mg and -Mg) cells <sup>a</sup>. The mean values of diameter and volume are also reported. The Mg concentrations assessed by DCHQ5, expressed in nmol/10<sup>6</sup> cells were normalized to the respective mean volume to obtain the molar concentrations. The p value is also reported.

<b>DCHQ5 (cells population analysis)</b>						
<b>Cellular Model</b>	<b>diameter</b>	<b>volume</b>	<b>volume</b>	<b>[Mg]</b>		
<b>HUVEC</b>	<b>(<math>\mu\text{m}</math>)</b>	<b>(<math>\mu\text{m}^3</math>)</b>	<b>(L)</b>	<b>(nmol/10<sup>6</sup> cells)</b>	<b>(mmol)</b>	<b>(mM)</b>
<b>Controls</b>	16.4	2266	2.27E-12	49.7	4.97E-11	<b>21.9</b>
				59.5	5.95E-11	<b>24.4</b>
				48.5	4.85E-11	<b>21.4</b>
				51.5	5.15E-11	<b>22.3</b>
<b>Mean</b>				<b>52.3</b>		<b>22.5</b>
<b>SD</b>				<b>4.3</b>		<b>1.1</b>
<b>CV</b>				8%		5%
<b>TRPM7 silenced</b>	16.3	2437	2.44E-12	51.8	5.18E-11	<b>21.2</b>
				56.0	5.60E-11	<b>25.2</b>
				49.7	4.97E-11	<b>22.8</b>
<b>Mean</b>				<b>52.5</b>		<b>23.1</b>
<b>SD</b>				<b>2.6</b>		<b>1.6</b>
<b>CV</b>				5%		7%
						<b>p value: 0.71</b>
<b>Cellular Model</b>	<b>diameter</b>	<b>volume</b>	<b>volume</b>	<b>[Mg]</b>		
<b>SaOS2</b>	<b>(<math>\mu\text{m}</math>)</b>	<b>(<math>\mu\text{m}^3</math>)</b>	<b>(L)</b>	<b>(nmol/10<sup>6</sup> cells)</b>	<b>(mmol)</b>	<b>(mM)</b>
<b>+ Mg</b>	16.6	2394	2.39E-12	30.1	3.01E-11	<b>13.35</b>
				34.0	3.40E-11	<b>15.07</b>
				29.2	2.92E-11	<b>12.95</b>
<b>Mean</b>				<b>31.1</b>		<b>13.8</b>
<b>SD</b>				<b>2.1</b>		<b>0.9</b>
<b>CV</b>				7%		7%
<b>- Mg</b>	16.5	1987	1.99E-12	15.6	1.56E-11	<b>7.6</b>
				18.5	1.85E-11	<b>9.1</b>
				15.7	1.57E-11	<b>7.7</b>
<b>Mean</b>				<b>16.6</b>		<b>8.1</b>
<b>SD</b>				<b>1.3</b>		<b>0.7</b>
<b>CV</b>				8%		8%
						<b>p value: 0.019</b>

<sup>a</sup> For each cell lines, the mean values of diameter and volume are also reported. The Mg concentrations assessed by DCHQ5, expressed in nmol/10<sup>6</sup> cells were normalized to the respective mean volume to obtain the molar concentrations. SD, standard deviation; CV, coefficient of variation, the value of the t-test is also reported.

**Table 5.6.** Molar concentration of Mg assessed by DCHQ5 in LoVo (sensitive and resistant) cells <sup>a</sup>. The mean values of diameter and volume are also reported. The Mg concentrations assessed by DCHQ5, expressed in nmol/10<sup>6</sup> cells were normalized to the respective mean volume to obtain the molar concentrations. The p value is also reported.

<b>DCHQ5 (cells population analysis)</b>						
<b>Cellular Model</b>	<b>diameter</b>	<b>volume</b>	<b>volume</b>	<b>[Mg]</b>		
<b>LoVo</b>	<b>(<math>\mu\text{m}</math>)</b>	<b>(<math>\mu\text{m}^3</math>)</b>	<b>(L)</b>	<b>(nmol/10<sup>6</sup> cells)</b>	<b>(mmol)</b>	<b>(mM)</b>
<b>Sensitive</b>	14.8	1713	1.71E-12	28.43	2.84E-11	<b>16.6</b>
				34.07	3.41E-11	<b>19.9</b>
				28.60	2.86E-11	<b>16.7</b>
				33.99	3.40E-11	<b>19.8</b>
				32.32	3.23E-11	<b>18.9</b>
				32.81	3.28E-11	<b>19.2</b>
				32.81	3.28E-11	<b>19.2</b>
				29.13	2.91E-11	<b>17.0</b>
<b>Mean</b>				<b>31.5</b>		<b>18.4</b>
<b>SD</b>				<b>2.2</b>		<b>1.3</b>
<b>CV</b>				<b>7%</b>		<b>7%</b>
<b>Resistant</b>	14.0	1423	1.42E-12	29.2	2.92E-11	<b>20.5</b>
				27.8	2.78E-11	<b>19.5</b>
				28.1	2.81E-11	<b>19.7</b>
				33.0	3.30E-11	<b>23.2</b>
				26.4	2.64E-11	<b>18.6</b>
				28.6	2.86E-11	<b>20.1</b>
				27.2	2.72E-11	<b>19.1</b>
				32.0	3.20E-11	<b>22.5</b>
<b>Mean</b>				<b>29.0</b>		<b>20.4</b>
<b>SD</b>				<b>2.1</b>		<b>1.5</b>
<b>CV</b>				<b>7%</b>		<b>7%</b>
						<b>p value: 0.009</b>

<sup>a</sup> For LoVo S and LoVo R the mean values of diameter and volume are also reported. The Mg concentrations assessed by DCHQ5, expressed in nmol/10<sup>6</sup> cells were normalized to the respective mean volume to obtain the molar concentrations.

SD, standard deviation; CV, coefficient of variation, the value of the t-test is also reported.

In the cell population analysis the TRPM7 silencing in HUVEC cells did not affected the Mg content respect to the controls, while the content of Mg was different both in LoVo, (p<0.05) and in SaOS2 cells, (p<0.05). In particular, DCHQ5 chemosensor shown a high sensibility detecting a small difference between sensitive (18.4±1.4

mM) and resistant ( $20.4 \pm 1.6$  mM) LoVo cells, denoting a small coefficient of variation (7%).

On the other hand, single cell analysis allow to reach the intracellular distribution of Mg but the technique is able to reveal only marked difference, as in the case of SaOS2 cells.

## **5.6 Single cell vs Cell population analyses**

An intrinsic limitation of the synchrotron-based fluorescence analyses is the reduction of the cellular volume that prevents the directly comparison of data of single cells with ones of cell population.

Indeed, in order to preserve the chemical integrity and morphology of the cells, we used cryogenic methods of fixation which, as well as all the other available methods of fixation, provoke a reduction of the cellular volume, mainly because of the loss of the intracellular H<sub>2</sub>O.

As a consequence, to compare the two approaches, we normalized the total magnesium concentration of each dehydrated cells calculated with single cells analysis with the mean volume of the corresponding cell population.

This normalization allowed us to compare the molar Mg concentrations of single cells with the concentration calculated using DCHQ5 (Fig 5.13).

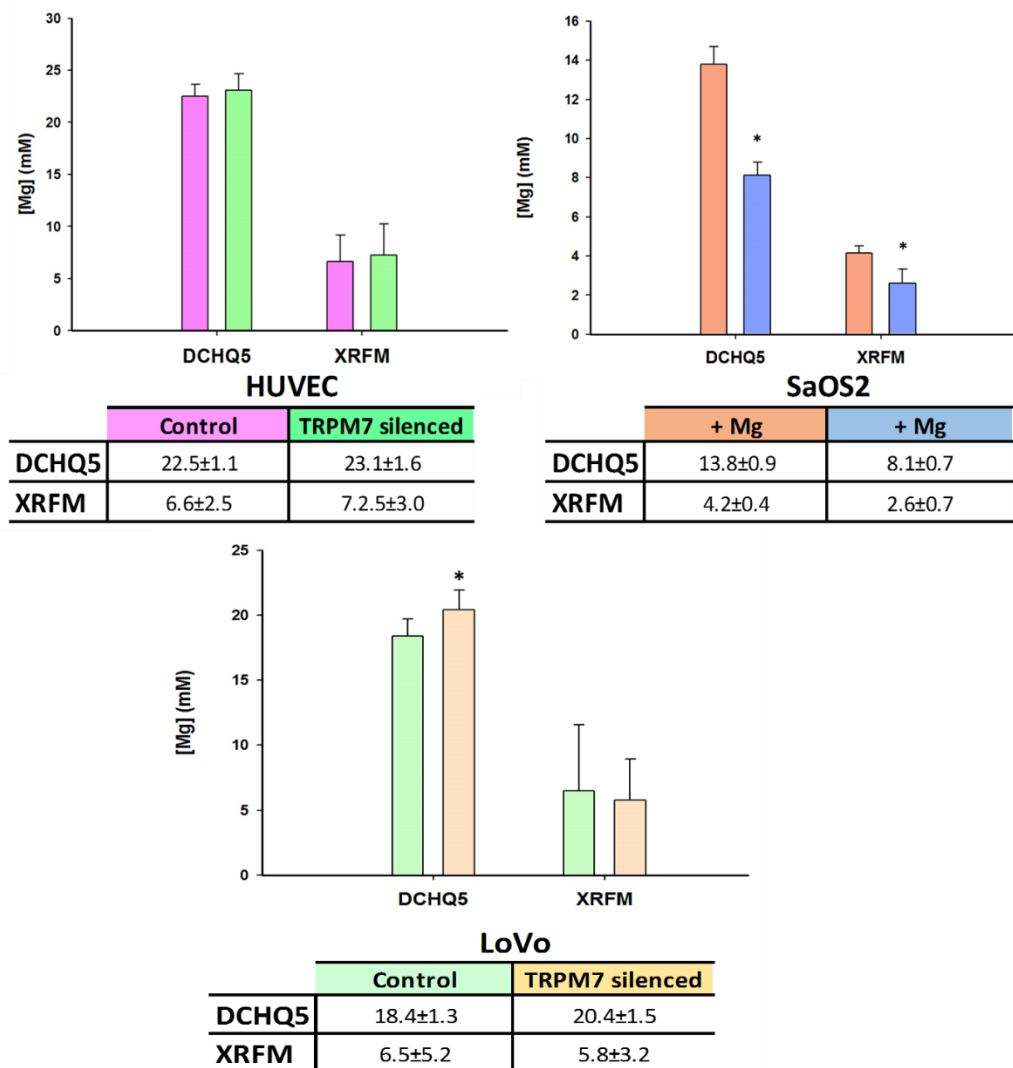


**Figure 5.13:** Comparison of Total Mg concentrations in treated and controls HUVEC (top on the left), SaOS2 (top on the right) and LoVo (bottom) cells, assessed by two different techniques: DCHQ5 spectrofluorimetric assay and XRFM multimodal approach. Magnesium intracellular concentration was evaluated by DCHQ5 fluorescence and synchrotron radiation referring to volume of the respective cell populations.

\* Significantly different from +Mg for SaOS2 cells and from LoVo S in LoVo cells,  $p < 0.05$ .

The results shown for all the three cell lines examined a smaller value using single cell analysis compare to cell population, but of the same order of magnitude.

Lastly, we calculated the ratio between the molar concentrations of Mg obtained with the two approach (Tab. 5.7).

**Table 5.7:** Ratio between the mean molar concentrations obtained by single cells and cell population analyses <sup>a</sup>

<b>Single cells / Cell population</b>		
	<b>CTRL</b>	<b>Treated</b>
<b>HUVEC</b>	0.29	0.31
<b>SaOS2</b>	0.3	0.32
<b>LoVo</b>	0.35	0.28

<sup>a</sup>CTRL indicate the mean molar concentration of control cells for HUVEC, of +Mg sample for SaOS cells, and of for LoVo S sample for LoVo cells; Treated indicate the mean molar concentration of TRPM7 silenced cells for HUVEC, of -Mg sample for SaOS cells, and of for LoVo R sample for LoVo cells.

It is worthy to note that the underestimation of single cells analyses is always of the same amount revealing a surprisingly constant number of about 0.3 for all the three cell lines.

## 6 CONCLUSIONS

Magnesium is one of the fundamental element for life, since it is still now recognized that biological processes strictly dependent on its availability, yet without a clear picture of its role. This is could be mainly due to the scarcity of versatile and sensitive analytical techniques.

The family of diaza-crown conjugated with two hydroxyquinoline arms represent a group of interesting dyes, where DCHQ5 is the most interestingly member, for a series of peculiar properties. In the study herein reported, we demonstrated that DCHQ5 is able to accurately quantify the total amount of Mg in a very "small" cellular population, of order of  $25\text{-}50 \times 10^3$  cells/mL, by using a simple spectrofluorimetric assay [146].

This unique analytical capability was fundamental for the investigation of the role of magnesium in the process of hASCs pre-commitment with a cocktail of know differentiating agents (HBR).

Furthermore, DCHQ5 demonstrated to be a versatile tool for different applications: its higher intracellular retentions allow to perform cytofluorimetric assays and two-photon confocal microscopy on whole and viable cells; its photochemical characteristic make it excitable in both UV and visible spectra, and the presence of different lifetimes allow to perform fluorescence life time imaging of intracellular Mg.

Combining this characteristic we demonstrated that DCHQ5 lifetimes distribution are homogeneous inside the cells, and the high fluorescence observed in the cellular membranes is not due a prevalence of the longer lifetime in the lipophilic environment but to a major concentration of the complex dye-Mg in these regions. These results support the hypothesis of the Rubin's theory about the signalling role of membrane bound magnesium [81]. In addictions, the high fluorescence at the perinuclear area is in agreements with the localization of magnesium store in mitochondria and endoplasmic reticulum [109], [133].

The performant analytical characteristic of DCHQ5, especially in terms of sensitivity, were further corroborate in the analyses of magnesium in multi drug resistance:

DCHQ5 was able to discriminate a very little but significant difference of magnesium among LoVo sensitive and resistant to doxorubicin [147].

Currently, DCHQ5 is the only one dye that possesses such accurate analytical characteristic, rendering this dye an important and fundamental tool for the study of magnesium homeostasis, especially when the poorly availability of samples is a limiting factor.

In these work we also exploited innovative techniques of x-ray fluorescence microscopy by using a multimodal approach in order to achieve within the cells the spatial distribution of the concentration of magnesium and fundamental light elements for life. The combination of classical and innovative analytical techniques can shed new light in the comprehension of magnesium homeostasis, since “how much” but also the more challenging “where is” are challenging but essential questions to answer.

In parallel, we also evaluated the role of magnesium in HBR pre-commitment of adipose derived mesenchymal stem cells.

We found that in normal magnesium availability, HBR-induced preconditioning of hASCs is associated by an increase of total magnesium content during time and by a block in the G2/M phase of the cell cycle.

Moreover, our results demonstrated that magnesium deprivation triggers a multilineage enrichments of HBR-induced preconditioning of hASCs, since the gene expression of several cell lineage markers are strongly enhanced when cells are grown in Mg-free medium.

This is extremely important because the possibility to easily obtain a higher yield of stem cells reactive to start different commitments only by combining HBR with magnesium deprivation, is proof of principle in regenerative medicine.

## REFERENCES

- [1] M. Barbagallo and L. J. Dominguez, "Magnesium metabolism in type 2 diabetes mellitus, metabolic syndrome and insulin resistance," *Arch. Biochem. Biophys.*, vol. 458, no. 1, pp. 40–47, Feb. 2007.
- [2] N. E. Saris, E. Mervaala, H. Karppanen, J. A. Khawaja, and A. Lewenstam, "Magnesium. An update on physiological, clinical and analytical aspects," *Clin. Chim. Acta Int. J. Clin. Chem.*, vol. 294, no. 1–2, pp. 1–26, Apr. 2000.
- [3] K. Kisters and U. Gröber, "Magnesium in health and disease," *Plant Soil*, vol. 368, no. 1–2, pp. 155–165, Apr. 2013.
- [4] J. H. F. de Baaij, J. G. J. Hoenderop, and R. J. M. Bindels, "Magnesium in Man: Implications for Health and Disease," *Physiol. Rev.*, vol. 95, no. 1, pp. 1–46, Jan. 2015.
- [5] L. Garfinkel and D. Garfinkel, "Magnesium regulation of the glycolytic pathway and the enzymes involved," *Magnesium*, vol. 4, no. 2–3, pp. 60–72, 1985.
- [6] U. Blaszczyk and A. Duda-Chodak, "Magnesium: its role in nutrition and carcinogenesis," *Rocz. Państw. Zakładu Hig.*, vol. 64, no. 3, pp. 165–171, 2013.
- [7] S. Long and A. M. Romani, "Role of Cellular Magnesium in Human Diseases," *Austin J. Nutr. Food Sci.*, vol. 2, no. 10, Nov. 2014.
- [8] J. H. F. de Baaij, J. G. J. Hoenderop, and R. J. M. Bindels, "Magnesium in Man: Implications for Health and Disease," *Physiol. Rev.*, vol. 95, no. 1, pp. 1–46, Jan. 2015.
- [9] A. M. P. Romani, "Magnesium Homeostasis in Mammalian Cells," in *Metallomics and the Cell*, L. Banci, Ed. Springer Netherlands, 2013, pp. 69–118.
- [10] C. de Rouffignac and G. Quamme, "Renal magnesium handling and its hormonal control," *Physiol. Rev.*, vol. 74, no. 2, pp. 305–322, Apr. 1994.
- [11] B. Raju, E. Murphy, L. A. Levy, R. D. Hall, and R. E. London, "A fluorescent indicator for measuring cytosolic free magnesium," *Am. J. Physiol. - Cell Physiol.*, vol. 256, no. 3, pp. C540–C548, Mar. 1989.
- [12] M. Fatholahi, K. LaNoue, A. Romani, and A. Scarpa, "Relationship between Total and Free Cellular Mg<sup>2+</sup> during Metabolic Stimulation of Rat Cardiac Myocytes and Perfused Hearts," *Arch. Biochem. Biophys.*, vol. 374, no. 2, pp. 395–401, Feb. 2000.
- [13] P. W. Flatman, "Mechanisms of Magnesium Transport," *Annu. Rev. Physiol.*, vol. 53, no. 1, pp. 259–271, 1991.

- [14] K. W. Beyenbach, "Transport of magnesium across biological membranes," *Magnes. Trace Elem.*, vol. 9, no. 5, pp. 233–254, 1990.
- [15] A. M. P. Romani, "Cellular magnesium homeostasis," *Arch. Biochem. Biophys.*, vol. 512, no. 1, pp. 1–23, Aug. 2011.
- [16] M. E. Maguire and J. A. Cowan, "Magnesium chemistry and biochemistry," *Biometals*, vol. 15, no. 3, pp. 203–210, Sep. 2002.
- [17] J. Sahni and A. M. Scharenberg, "The SLC41 family of MgtE-like magnesium transporters," *Mol. Aspects Med.*, vol. 34, no. 2–3, pp. 620–628, Apr. 2013.
- [18] M. Kolisek, A. Nestler, J. Vormann, and M. Schweigel-Röntgen, "Human gene SLC41A1 encodes for the Na<sup>+</sup>/Mg<sup>2+</sup> exchanger," *Am. J. Physiol. Cell Physiol.*, vol. 302, no. 1, pp. C318–326, Jan. 2012.
- [19] A. Fleig and R. Penner, "The TRPM ion channel subfamily: molecular, biophysical and functional features," *Trends Pharmacol. Sci.*, vol. 25, no. 12, pp. 633–639, Dec. 2004.
- [20] C. Montell, "Mg<sup>2+</sup> Homeostasis: The Mg<sup>2+</sup>-nificant TRPM Chanzymes," *Curr. Biol.*, vol. 13, no. 20, pp. R799–R801, Oct. 2003.
- [21] S. W. Crawley and G. P. Côté, "Identification of dimer interactions required for the catalytic activity of the TRPM7 alpha-kinase domain," *Biochem. J.*, vol. 420, no. 1, pp. 115–122, May 2009.
- [22] C. Schmitz, M. V. Dorovkov, X. Zhao, B. J. Davenport, A. G. Ryazanov, and A.-L. Perraud, "The Channel Kinases TRPM6 and TRPM7 Are Functionally Nonredundant," *J. Biol. Chem.*, vol. 280, no. 45, pp. 37763–37771, Nov. 2005.
- [23] K. P. Schlingmann, S. Waldegger, M. Konrad, V. Chubanov, and T. Gudermann, "TRPM6 and TRPM7—Gatekeepers of human magnesium metabolism," *Biochim. Biophys. Acta BBA - Mol. Basis Dis.*, vol. 1772, no. 8, pp. 813–821, Aug. 2007.
- [24] K. Brandao, F. Deason-Towne, A.-L. Perraud, and C. Schmitz, "The role of Mg<sup>2+</sup> in immune cells," *Immunol. Res.*, vol. 55, no. 1–3, pp. 261–269, Mar. 2013.
- [25] K. P. Schlingmann, S. Weber, M. Peters, L. Niemann Nejsum, H. Vitzthum, K. Klingel, M. Kratz, E. Haddad, E. Ristoff, D. Dinour, M. Syrrou, S. Nielsen, M. Sassen, S. Waldegger, H. W. Seyberth, and M. Konrad, "Hypomagnesemia with secondary hypocalcemia is caused by mutations in TRPM6, a new member of the TRPM gene family," *Nat. Genet.*, vol. 31, no. 2, pp. 166–170, Jun. 2002.
- [26] R. Y. Walder, D. Landau, P. Meyer, H. Shalev, M. Tsolia, Z. Borochowitz, M. B. Boettger, G. E. Beck, R. K. Englehardt, R. Carmi, and V. C. Sheffield, "Mutation of TRPM6 causes familial hypomagnesemia with secondary hypocalcemia," *Nat. Genet.*, vol. 31, no. 2, pp. 171–174, Jun. 2002.

- [27] K. Brandao, F. Deason-Towne, X. Zhao, A.-L. Perraud, and C. Schmitz, "TRPM6 kinase activity regulates TRPM7 trafficking and inhibits cellular growth under hypomagnesic conditions," *Cell. Mol. Life Sci. CMLS*, vol. 71, no. 24, pp. 4853–4867, Dec. 2014.
- [28] C. Schmitz, A.-L. Perraud, C. O. Johnson, K. Inabe, M. K. Smith, R. Penner, T. Kurosaki, A. Fleig, and A. M. Scharenberg, "Regulation of vertebrate cellular  $Mg^{2+}$  homeostasis by TRPM7," *Cell*, vol. 114, no. 2, pp. 191–200, Jul. 2003.
- [29] T. E. Woudenberg-Vrenken, A. Sukinta, A. W. van der Kemp, R. J. M. Bindels, and J. G. J. Hoenderop, "Transient receptor potential melastatin 6 knockout mice are lethal whereas heterozygous deletion results in mild hypomagnesemia," *Nephron Physiol.*, vol. 117, no. 2, pp. p11–19, 2011.
- [30] L. V. Ryazanova, L. J. Rondon, S. Zierler, Z. Hu, J. Galli, T. P. Yamaguchi, A. Mazur, A. Fleig, and A. G. Ryazanov, "TRPM7 is essential for  $Mg(2+)$  homeostasis in mammals," *Nat. Commun.*, vol. 1, p. 109, 2010.
- [31] I. Dhennin-Duthille, M. Gautier, I. Korichneva, and H. Ouadid-Ahidouch, "TRPM7 involvement in cancer: A potential prognostic factor," *Magnes. Res.*, vol. 27, no. 3, pp. 103–112, 2014.
- [32] G. A. Quamme, "Molecular identification of ancient and modern mammalian magnesium transporters," *Am. J. Physiol. - Cell Physiol.*, vol. 298, no. 3, pp. C407–C429, Mar. 2010.
- [33] H. Zhou and D. E. Clapham, "Mammalian MagT1 and TUSC3 are required for cellular magnesium uptake and vertebrate embryonic development," *Proc. Natl. Acad. Sci. U. S. A.*, vol. 106, no. 37, pp. 15750–15755, Sep. 2009.
- [34] F. Deason-Towne, A.-L. Perraud, and C. Schmitz, "The  $Mg^{2+}$  transporter MagT1 partially rescues cell growth and  $Mg^{2+}$  uptake in cells lacking the channel-kinase TRPM7," *FEBS Lett.*, vol. 585, no. 14, pp. 2275–2278, Jul. 2011.
- [35] J. Ravell, B. Chaigne-Delalande, and M. Lenardo, "X-linked immunodeficiency with magnesium defect, Epstein-Barr virus infection, and neoplasia disease: a combined immune deficiency with magnesium defect," *Curr. Opin. Pediatr.*, vol. 26, no. 6, pp. 713–719, Dec. 2014.
- [36] C. Schmitz, F. Deason, and A.-L. Perraud, "Molecular components of vertebrate  $Mg^{2+}$ -homeostasis regulation," *Magnes. Res. Off. Organ Int. Soc. Dev. Res. Magnes.*, vol. 20, no. 1, pp. 6–18, Mar. 2007.
- [37] J. Hou, A. Renigunta, A. S. Gomes, M. Hou, D. L. Paul, S. Waldegger, and D. A. Goodenough, "Claudin-16 and claudin-19 interaction is required for their assembly into tight junctions and for renal reabsorption of magnesium," *Proc. Natl. Acad. Sci. U. S. A.*, vol. 106, no. 36, pp. 15350–15355, Sep. 2009.

- [38] C.-Y. Wang, J.-D. Shi, P. Yang, P. G. Kumar, Q.-Z. Li, Q.-G. Run, Y.-C. Su, H. S. Scott, K.-J. Kao, and J.-X. She, "Molecular cloning and characterization of a novel gene family of four ancient conserved domain proteins (ACDP)," *Gene*, vol. 306, pp. 37–44, Mar. 2003.
- [39] I. Gómez-García, M. Stuiver, J. Ereño, I. Oyenarte, M. A. Corral-Rodríguez, D. Müller, and L. A. Martínez-Cruz, "Purification, crystallization and preliminary crystallographic analysis of the CBS-domain pair of cyclin M2 (CNNM2)," *Acta Crystallograph. Sect. F Struct. Biol. Cryst. Commun.*, vol. 68, no. Pt 10, pp. 1198–1203, Sep. 2012.
- [40] J. H. F. de Baaij, M. Stuiver, I. C. Meij, S. Lainez, K. Kopplin, H. Venselaar, D. Müller, R. J. M. Bindels, and J. G. J. Hoenderop, "Membrane Topology and Intracellular Processing of Cyclin M2 (CNNM2)," *J. Biol. Chem.*, vol. 287, no. 17, pp. 13644–13655, Apr. 2012.
- [41] M. Stuiver, S. Lainez, C. Will, S. Terry, D. Günzel, H. Debaix, K. Sommer, K. Kopplin, J. Thumfart, N. B. Kampik, U. Querfeld, T. E. Willnow, V. Němec, C. A. Wagner, J. G. Hoenderop, O. Devuyst, N. V. A. M. Knoers, R. J. Bindels, I. C. Meij, and D. Müller, "CNNM2, Encoding a Basolateral Protein Required for Renal Mg<sup>2+</sup> Handling, Is Mutated in Dominant Hypomagnesemia," *Am. J. Hum. Genet.*, vol. 88, no. 3, pp. 333–343, Mar. 2011.
- [42] T. E. Meyer, G. C. Verwoert, S.-J. Hwang, N. L. Glazer, A. V. Smith, F. J. A. van Rooij, G. B. Ehret, E. Boerwinkle, J. F. Felix, T. S. Leak, T. B. Harris, Q. Yang, A. Dehghan, T. Aspelund, R. Katz, G. Homuth, T. Kocher, R. Rettig, J. S. Ried, C. Gieger, H. Prucha, A. Pfeufer, T. Meitinger, J. Coresh, A. Hofman, M. J. Sarnak, Y.-D. I. Chen, A. G. Uitterlinden, A. Chakravarti, B. M. Psaty, C. M. van Duijn, W. H. L. Kao, J. C. M. Witteman, V. Gudnason, D. S. Siscovick, C. S. Fox, A. Köttgen, The Genetic Factors for Osteoporosis (GEFOS) Consortium, and Meta Analysis of Glucose and Insulin Related Traits Consortium (MAGIC), "Genome-Wide Association Studies of Serum Magnesium, Potassium, and Sodium Concentrations Identify Six Loci Influencing Serum Magnesium Levels," *PLoS Genet*, vol. 6, no. 8, p. e1001045, Aug. 2010.
- [43] S. Hardy, N. Uetani, N. Wong, E. Kostantin, D. P. Labbé, L. R. Bégin, A. Mes-Masson, D. Miranda-Saavedra, and M. L. Tremblay, "The protein tyrosine phosphatase PRL-2 interacts with the magnesium transporter CNNM3 to promote oncogenesis," *Oncogene*, vol. 34, no. 8, pp. 986–995, Feb. 2015.
- [44] M. Piskacek, L. Zotova, G. Zsurka, and R. J. Schweyen, "Conditional knockdown of hMRS2 results in loss of mitochondrial Mg(2+) uptake and cell death," *J. Cell. Mol. Med.*, vol. 13, no. 4, pp. 693–700, Apr. 2009.
- [45] M. Kolisek, G. Zsurka, J. Samaj, J. Weghuber, R. J. Schweyen, and M. Schweigel, "Mrs2p is an essential component of the major electrophoretic Mg<sup>2+</sup> influx system in mitochondria," *EMBO J.*, vol. 22, no. 6, pp. 1235–1244, Mar. 2003.

- [46] Y. Chen, X. Wei, P. Yan, Y. Han, S. Sun, K. Wu, and D. Fan, "Human mitochondrial Mrs2 protein promotes multidrug resistance in gastric cancer cells by regulating p27, cyclin D1 expression and cytochrome C release," *Cancer Biol. Ther.*, vol. 8, no. 7, pp. 607–614, Apr. 2009.
- [47] F. I. Wolf and V. Trapani, "Multidrug resistance phenotypes and MRS2 mitochondrial magnesium channel: Two players from one stemness?," *Cancer Biol. Ther.*, vol. 8, no. 7, 2009.
- [48] L. Banci, *Metallomics and the Cell*. Springer Science & Business Media, 2013.
- [49] R. Ishitani, Y. Sugita, N. Dohmae, N. Furuya, M. Hattori, and O. Nureki, "Mg<sup>2+</sup>-sensing mechanism of Mg<sup>2+</sup> transporter MgtE probed by molecular dynamics study," *Proc. Natl. Acad. Sci. U. S. A.*, vol. 105, no. 40, pp. 15393–15398, Oct. 2008.
- [50] M. Hattori, N. Iwase, N. Furuya, Y. Tanaka, T. Tsukazaki, R. Ishitani, M. E. Maguire, K. Ito, A. Maturana, and O. Nureki, "Mg<sup>2+</sup>-dependent gating of bacterial MgtE channel underlies Mg<sup>2+</sup> homeostasis," *EMBO J.*, vol. 28, no. 22, pp. 3602–3612, Nov. 2009.
- [51] M. Hattori, Y. Tanaka, S. Fukai, R. Ishitani, and O. Nureki, "Crystal structure of the MgtE Mg<sup>2+</sup> transporter," *Nature*, vol. 448, no. 7157, pp. 1072–1075, Aug. 2007.
- [52] A. Fleig, M. Schweigel-Röntgen, and M. Kolisek, "Solute Carrier Family SLC41, what do we really know about it?," *Wiley Interdiscip. Rev. Membr. Transp. Signal.*, vol. 2, no. 6, 2013.
- [53] A. Tucci, M. A. Nalls, H. Houlden, T. Revesz, A. B. Singleton, N. W. Wood, J. Hardy, and C. Paisán-Ruiz, "Genetic variability at the PARK16 locus," *Eur. J. Hum. Genet. EJHG*, vol. 18, no. 12, pp. 1356–1359, Dec. 2010.
- [54] Y. Yan, J. Tian, X. Mo, G. Zhao, X. Yin, J. Pu, and B. Zhang, "Genetic variants in the RAB7L1 and SLC41A1 genes of the PARK16 locus in Chinese Parkinson's disease patients," *Int. J. Neurosci.*, vol. 121, no. 11, pp. 632–636, Nov. 2011.
- [55] M. Kolisek, G. Sponder, L. Mastrototaro, A. Smorodchenko, P. Launay, J. Vormann, and M. Schweigel-Röntgen, "Substitution p.A350V in Na<sup>+</sup>/Mg<sup>2+</sup> Exchanger SLC41A1, Potentially Associated with Parkinson's Disease, Is a Gain-of-Function Mutation," *PLoS ONE*, vol. 8, no. 8, p. e71096, Aug. 2013.
- [56] A. Romani, C. Marfella, and A. Scarpa, "Regulation of magnesium uptake and release in the heart and in isolated ventricular myocytes," *Circ. Res.*, vol. 72, no. 6, pp. 1139–1148, Jun. 1993.
- [57] D. L. Hwang, C. F. Yen, and J. L. Nadler, "Insulin increases intracellular magnesium transport in human platelets," *J. Clin. Endocrinol. Metab.*, vol. 76, no. 3, pp. 549–553, Mar. 1993.

- [58] T. Günther, "Mechanisms and regulation of  $Mg^{2+}$  efflux and  $Mg^{2+}$  influx," *Miner. Electrolyte Metab.*, vol. 19, no. 4–5, pp. 259–265, 1993.
- [59] A. Romani and A. Scarpa, "Hormonal control of  $Mg^{2+}$  transport in the heart," *Nature*, vol. 346, no. 6287, pp. 841–844, Aug. 1990.
- [60] T. Günther and J. Vormann, "Na(+)-dependent  $Mg^{2+}$  efflux from Mg(2+)-loaded rat thymocytes and HL 60 cells.," *Magnes. Trace Elem.*, vol. 9, no. 5, pp. 279–282, 1990.
- [61] G. Rd and M. Me, "Magnesium as a regulatory cation: criteria and evaluation.," *Magnesium*, vol. 6, no. 3, pp. 113–127, Dec. 1986.
- [62] T. E. Fagan and A. Romani, " $\alpha$ 1-Adrenoceptor-induced  $Mg^{2+}$  extrusion from rat hepatocytes occurs via Na+-dependent transport mechanism," *Am. J. Physiol. - Gastrointest. Liver Physiol.*, vol. 280, no. 6, pp. G1145–G1156, Jun. 2001.
- [63] J. J. Erdos and M. E. Maguire, "Hormone-sensitive magnesium transport in murine S49 lymphoma cells: characterization and specificity for magnesium," *J. Physiol.*, vol. 337, no. 1, pp. 351–371, Apr. 1983.
- [64] T. Günther and J. Vormann, "Reversibility of  $Na^+/Mg^{2+}$  antiport in rat erythrocytes," *Biochim. Biophys. Acta BBA - Biomembr.*, vol. 1234, no. 1, pp. 105–110, Mar. 1995.
- [65] R. M. Touyz and G. Yao, "Modulation of vascular smooth muscle cell growth by magnesium—role of mitogen—activated protein kinases," *J. Cell. Physiol.*, vol. 197, no. 3, pp. 326–335, Dec. 2003.
- [66] A. Ikari, A. Sanada, C. Okude, H. Sawada, Y. Yamazaki, J. Sugatani, and M. Miwa, "Up-regulation of TRPM6 transcriptional activity by AP-1 in renal epithelial cells," *J. Cell. Physiol.*, vol. 222, no. 3, pp. 481–487, Mar. 2010.
- [67] D. Cunningham, Y. Humblet, S. Siena, D. Khayat, H. Bleiberg, A. Santoro, D. Bets, M. Mueser, A. Harstrick, C. Verslype, I. Chau, and E. Van Cutsem, "Cetuximab Monotherapy and Cetuximab plus Irinotecan in Irinotecan-Refractory Metastatic Colorectal Cancer," *N. Engl. J. Med.*, vol. 351, no. 4, pp. 337–345, Jul. 2004.
- [68] H. Dimke, J. van der Wijst, T. R. Alexander, I. M. J. Meijer, G. M. Mulder, H. van Goor, S. Tejpar, J. G. Hoenderop, and R. J. Bindels, "Effects of the EGFR Inhibitor Erlotinib on Magnesium Handling," *J. Am. Soc. Nephrol. JASN*, vol. 21, no. 8, pp. 1309–1316, Aug. 2010.
- [69] J. A. (James A. ) Cowan, *Biological chemistry of magnesium*. VCH Publishers, 1995.

- [70] F. I. Wolf, V. Trapani, and A. Cittadini, "Magnesium and the control of cell proliferation: Looking for a needle in a haystack," *Magnes. Res.*, vol. 21, no. 2, pp. 83–91, 2008.
- [71] F. I. Wolf and V. Trapani, "Cell (patho)physiology of magnesium," *Clin. Sci.*, vol. 114, no. 1, pp. 27–35, Jan. 2008.
- [72] F. I. Wolf, S. Fasanella, B. Tedesco, A. Torsello, A. Sgambato, B. Faraglia, P. Palozza, A. Boninsegna, and A. Cittadini, "Regulation of magnesium content during proliferation of mammary epithelial cells (HC-11).," *Front. Biosci. J. Virtual Libr.*, vol. 9, pp. 2056–2062, 2004.
- [73] S. Ferrè, A. Mazur, and J. A. M. Maier, "Low-magnesium induces senescent features in cultured human endothelial cells," *Magnes. Res.*, vol. 20, no. 1, pp. 66–71, 2007.
- [74] D. W. Killilea and B. N. Ames, "Magnesium deficiency accelerates cellular senescence in cultured human fibroblasts," *Proc. Natl. Acad. Sci.*, vol. 105, no. 15, pp. 5768–5773, Apr. 2008.
- [75] A. Sgambato, F. I. Wolf, B. Faraglia, and A. Cittadini, "Magnesium depletion causes growth inhibition, reduced expression of cyclin D1, and increased expression of P27KIP1 in normal but not in transformed mammary epithelial cells," *J. Cell. Physiol.*, vol. 180, no. 2, pp. 245–254, Aug. 1999.
- [76] V. Covacci, N. Bruzzese, A. Sgambato, A. Di Francesco, M. A. Russo, F. I. Wolf, and A. Cittadini, "Magnesium restriction induces granulocytic differentiation and expression of P27Kip1 in human leukemic HL-60 cells," *J. Cell. Biochem.*, vol. 70, no. 3, pp. 313–322, Sep. 1998.
- [77] Maier JAM, Nasulewicz-Goldeman A, Simonacci M, Boninsegna A, Mazur A, and Wolf FI, "Insights Into the Mechanisms Involved in Magnesium-Dependent Inhibition of Primary Tumor Growth," *Nutr. Cancer*, vol. 59, no. 2, pp. 192–198 7p, Nov. 2007.
- [78] A. Nasulewicz, J. Wietrzyk, F. I. Wolf, S. Dzimira, J. Madej, J. A. M. Maier, Y. Rayssiguier, A. Mazur, and A. Opolski, "Magnesium deficiency inhibits primary tumor growth but favors metastasis in mice," *Biochim. Biophys. Acta BBA - Mol. Basis Dis.*, vol. 1739, no. 1, pp. 26–32, Dec. 2004.
- [79] D. Bernardini, "Magnesium and microvascular endothelial cells: a role in inflammation and angiogenesis," *Front. Biosci.*, vol. 10, no. 1–3, p. 1177, 2005.
- [80] A. Sgambato, B. Faraglia, R. Ardito, A. Torsello, A. Boninsegna, A. Cittadini, and F. I. Wolf, "Isolation of Normal Epithelial Cells Adapted to Grow at Nonphysiological Concentration of Magnesium," *Biochem. Biophys. Res. Commun.*, vol. 286, no. 4, pp. 752–757, Aug. 2001.

- [81] H. Rubin, "The membrane, magnesium, mitosis (MMM) model of cell proliferation control," *Magnes. Res.*, vol. 18, no. 4, pp. 268–274, Dec. 2005.
- [82] H. Rubin, "Magnesium: The missing element in molecular views of cell proliferation control," *BioEssays*, vol. 27, no. 3, pp. 311–320, Mar. 2005.
- [83] S. Castiglioni, M. Leidi, E. Carpanese, and J. A. M. Maier, "Extracellular magnesium and in vitro cell differentiation: Different behaviour of different cells," *Magnes. Res.*, vol. 26, no. 1, pp. 24–31, 2013.
- [84] F. I. Wolf and A. Cittadini, "Magnesium in cell proliferation and differentiation.," *Front. Biosci. J. Virtual Libr.*, vol. 4, pp. D607–617, 1999.
- [85] A. Di Francesco, R. W. Desnoyer, V. Covacci, F. I. Wolf, A. Romani, A. Cittadini, and M. Bond, "Changes in Magnesium Content and Subcellular Distribution during Retinoic Acid-Induced Differentiation of HL60 Cells," *Arch. Biochem. Biophys.*, vol. 360, no. 2, pp. 149–157, Dec. 1998.
- [86] H. Rubin, C. Vidair, and H. Sanui, "Restoration of normal appearance, growth behavior, and calcium content to transformed 3T3 cells by magnesium deprivation," *Proc. Natl. Acad. Sci.*, vol. 78, no. 4, pp. 2350–2354, Apr. 1981.
- [87] Y. Furutani, M. Funaba, and T. Matsui, "Magnesium deficiency up-regulates Myod expression in rat skeletal muscle and C2C12 myogenic cells," *Cell Biochem. Funct.*, vol. 29, no. 7, pp. 577–581, Oct. 2011.
- [88] M. Leidi, F. Delleria, M. Mariotti, and J. A. M. Maier, "High magnesium inhibits human osteoblast differentiation in vitro," *Magnes. Res.*, vol. 24, no. 1, pp. 1–6, 2011.
- [89] S. Nakatani, H. Mano, I. M. Ryanghyok, J. Shimizu, and M. Wada, "Excess magnesium inhibits excess calcium-induced matrix-mineralization and production of matrix gla protein (MGP) by ATDC5 cells," *Biochem. Biophys. Res. Commun.*, vol. 348, no. 3, pp. 1157–1162, Sep. 2006.
- [90] V. Hoftiezer, P.-O. Berggren, and B. Hellman, "Effects of altered  $\text{Ca}^{2+}$  and  $\text{Mg}^{2+}$  concentrations on proliferation and functional differentiation of the clonal insulin-producing cells RINm5F," *Cancer Lett.*, vol. 27, no. 1, pp. 7–14, May 1985.
- [91] A. M. P. Romani, "Magnesium Homeostasis in Mammalian Cells," in *Metallomics and the Cell*, L. Banci, Ed. Springer Netherlands, 2013, pp. 69–118.
- [92] V. Trapani, G. Farruggia, C. Marraccini, S. Iotti, A. Cittadini, and F. I. Wolf, "Intracellular magnesium detection: imaging a brighter future," *The Analyst*, vol. 135, no. 8, p. 1855, 2010.

- [93] X. Hou and B. T. Jones, "Inductively Coupled Plasma-Optical Emission Spectrometry," in *Encyclopedia of Analytical Chemistry*, John Wiley & Sons, Ltd, 2006.
- [94] D. L. Tsalev and V. I. Slaveykova, "Chemical modification in electrothermal atomic absorption spectrometry. Organization and classification of data by multivariate methods. Invited lecture," *J. Anal. At. Spectrom.*, vol. 7, no. 2, pp. 147–153, Jan. 1992.
- [95] S. Iotti, C. Frassinetti, L. Alderighi, A. Sabatini, A. Vacca, and B. Barbiroli, "In vivo  $^{31}\text{P}$ -MRS assessment of cytosolic  $[\text{Mg}^{2+}]$  in the human skeletal muscle in different metabolic conditions," *Magn. Reson. Imaging*, vol. 18, no. 5, pp. 607–614, Jun. 2000.
- [96] S. Iotti, C. Frassinetti, L. Alderighi, A. Sabatini, A. Vacca, and B. Barbiroli, "In vivo assessment of free magnesium concentration in human brain by  $^{31}\text{P}$  MRS. A new calibration curve based on a mathematical algorithm," *NMR Biomed.*, vol. 9, no. 1, pp. 24–32, Feb. 1996.
- [97] H. J. Huijgen, R. Sanders, S. A. Cecco, N. N. Rehak, G. T. Sanders, and R. J. Elin, "Serum Ionized Magnesium: Comparison of Results Obtained with Three Ion-Selective Analyzers," *Clin. Chem. Lab. Med.*, vol. 37, no. 4, pp. 465–470, 2005.
- [98] D. Günzel and W.-R. Schlue, "Determination of  $[\text{Mg}(2+)]_i$  - an update on the use of  $\text{Mg}(2+)$ -selective electrodes," *Biometals Int. J. Role Met. Ions Biol. Biochem. Med.*, vol. 15, no. 3, pp. 237–249, Sep. 2002.
- [99] R. K. Gupta, J. L. Benovic, and Z. B. Rose, "The determination of the free magnesium level in the human red blood cell by  $^{31}\text{P}$  NMR," *J. Biol. Chem.*, vol. 253, no. 17, pp. 6172–6176, Sep. 1978.
- [100] M. Bond, G. Vadasz, A. V. Somlyo, and A. P. Somlyo, "Subcellular calcium and magnesium mobilization in rat liver stimulated in vivo with vasopressin and glucagon," *J. Biol. Chem.*, vol. 262, no. 32, pp. 15630–15636, Nov. 1987.
- [101] F. I. Wolf, A. Torsello, S. Fasanella, and A. Cittadini, "Cell physiology of magnesium," *Mol. Aspects Med.*, vol. 24, no. 1–3, pp. 11–26, Jun. 2003.
- [102] R. P. Haugland, *Handbook of fluorescent probes and research products*. Molecular Probes, 2002.
- [103] H. Komatsu, N. Iwasawa, D. Citterio, Y. Suzuki, T. Kubota, K. Tokuno, Y. Kitamura, K. Oka, and K. Suzuki, "Design and Synthesis of Highly Sensitive and Selective Fluorescein-Derived Magnesium Fluorescent Probes and Application to Intracellular 3D  $\text{Mg}^{2+}$  Imaging," *J. Am. Chem. Soc.*, vol. 126, no. 50, pp. 16353–16360, Dec. 2004.

- [104] G. Grynkiewicz, M. Poenie, and R. Y. Tsien, "A new generation of  $\text{Ca}^{2+}$  indicators with greatly improved fluorescence properties," *J. Biol. Chem.*, vol. 260, no. 6, pp. 3440–3450, Mar. 1985.
- [105] R. Y. Tsien, "New calcium indicators and buffers with high selectivity against magnesium and protons: design, synthesis, and properties of prototype structures," *Biochemistry (Mosc.)*, vol. 19, no. 11, pp. 2396–2404, May 1980.
- [106] L. Basabe-Desmonts, D. N. Reinhoudt, and M. Crego-Calama, "Design of fluorescent materials for chemical sensing," *Chem. Soc. Rev.*, vol. 36, no. 6, pp. 993–1017, May 2007.
- [107] L. A. Levy, E. Murphy, B. Raju, and R. E. London, "Measurement of cytosolic free magnesium ion concentration by fluorine-19 NMR," *Biochemistry (Mosc.)*, vol. 27, no. 11, pp. 4041–4048, May 1988.
- [108] Y. Suzuki, H. Komatsu, T. Ikeda, N. Saito, S. Araki, D. Citterio, H. Hisamoto, Y. Kitamura, T. Kubota, J. Nakagawa, K. Oka, and K. Suzuki, "Design and Synthesis of  $\text{Mg}^{2+}$ -Selective Fluoroionophores Based on a Coumarin Derivative and Application for  $\text{Mg}^{2+}$  Measurement in a Living Cell," *Anal. Chem.*, vol. 74, no. 6, pp. 1423–1428, Mar. 2002.
- [109] T. Kubota, Y. Shindo, K. Tokuno, H. Komatsu, H. Ogawa, S. Kudo, Y. Kitamura, K. Suzuki, and K. Oka, "Mitochondria are intracellular magnesium stores: investigation by simultaneous fluorescent imagings in PC12 cells," *Biochim. Biophys. Acta BBA - Mol. Cell Res.*, vol. 1744, no. 1, pp. 19–28, May 2005.
- [110] Y. Shindo, T. Fujii, H. Komatsu, D. Citterio, K. Hotta, K. Suzuki, and K. Oka, "Newly Developed  $\text{Mg}^{2+}$ -Selective Fluorescent Probe Enables Visualization of  $\text{Mg}^{2+}$  Dynamics in Mitochondria," *PLoS ONE*, vol. 6, no. 8, p. e23684, Aug. 2011.
- [111] T. Fujii, Y. Shindo, K. Hotta, D. Citterio, S. Nishiyama, K. Suzuki, and K. Oka, "Design and Synthesis of a FlAsH-Type  $\text{Mg}^{2+}$  Fluorescent Probe for Specific Protein Labeling," *J. Am. Chem. Soc.*, vol. 136, no. 6, pp. 2374–2381, Feb. 2014.
- [112] H. Komatsu, T. Miki, D. Citterio, T. Kubota, Y. Shindo, Y. Kitamura, K. Oka, and K. Suzuki, "Single Molecular Multianalyte ( $\text{Ca}^{2+}$ ,  $\text{Mg}^{2+}$ ) Fluorescent Probe and Applications to Bioimaging," *J. Am. Chem. Soc.*, vol. 127, no. 31, pp. 10798–10799, Aug. 2005.
- [113] H. M. Kim, C. Jung, B. R. Kim, S.-Y. Jung, J. H. Hong, Y.-G. Ko, K. J. Lee, and B. R. Cho, "Environment-Sensitive Two-Photon Probe for Intracellular Free Magnesium Ions in Live Tissue," *Angew. Chem. Int. Ed.*, vol. 46, no. 19, pp. 3460–3463, May 2007.
- [114] C. Marraccini, G. Farruggia, M. Lombardo, L. Prodi, M. Sgarzi, V. Trapani, C. Trombini, F. I. Wolf, N. Zaccheroni, and S. Iotti, "Diaza-18-crown-6 hydroxyquinoline derivatives as flexible tools for the assessment and imaging

of total intracellular magnesium,” *Chem. Sci.*, vol. 3, no. 3, pp. 727–734, Feb. 2012.

- [115] G. Farruggia, S. Iotti, L. Prodi, M. Montalti, N. Zaccheroni, P. B. Savage, V. Trapani, P. Sale, and F. I. Wolf, “8-Hydroxyquinoline Derivatives as Fluorescent Sensors for Magnesium in Living Cells,” *J. Am. Chem. Soc.*, vol. 128, no. 1, pp. 344–350, Jan. 2006.
- [116] K. Soroka, R. S. Vithanage, D. A. Phillips, B. Walker, and P. K. Dasgupta, “Fluorescence properties of metal complexes of 8-hydroxyquinoline-5-sulfonic acid and chromatographic applications,” *Anal. Chem.*, vol. 59, no. 4, pp. 629–636, Feb. 1987.
- [117] L. Prodi, M. Montalti, J. S. Bradshaw, R. M. Izatt, and P. B. Savage, “Dependence on pH of the Luminescent Properties of Metal Ion Complexes of 5-Chloro-8-hydroxyquinoline Appended Diaza-18-Crown-6,” *J. Incl. Phenom. Macrocycl. Chem.*, vol. 41, no. 1–4, pp. 123–127, Dec. 2001.
- [118] I. Devol and E. Bardez, “Complexation of Al(III) by 8-Hydroxyquinoline and Drastic Fluorescence Enhancement in Reverse Micelles,” *J. Colloid Interface Sci.*, vol. 200, no. 2, pp. 241–248, Apr. 1998.
- [119] L. Prodi, F. Bolletta, M. Montalti, N. Zaccheroni, P. B. Savage, J. S. Bradshaw, and R. M. Izatt, “A fluorescent sensor for magnesium ions,” *Tetrahedron Lett.*, vol. 39, no. 31, pp. 5451–5454, Jul. 1998.
- [120] G. Farruggia, S. Iotti, L. Prodi, N. Zaccheroni, M. Montalti, P. B. Savage, G. Andreani, V. Trapani, and F. I. Wolf, “A Simple Spectrofluorometric Assay to Measure Total Intracellular Magnesium by a Hydroxyquinoline Derivative,” *J. Fluoresc.*, vol. 19, no. 1, pp. 11–19, Jun. 2008.
- [121] S. M. Kaiser and B. I. Escher, “The Evaluation of Liposome-Water Partitioning of 8-Hydroxyquinolines and Their Copper Complexes,” *Environ. Sci. Technol.*, vol. 40, no. 6, pp. 1784–1791, Mar. 2006.
- [122] G. Farruggia, S. Iotti, M. Lombardo, C. Marraccini, D. Petruzzello, L. Prodi, M. Sgarzi, C. Trombini, and N. Zaccheroni, “Microwave Assisted Synthesis of a Small Library of Substituted N,N’-Bis((8-hydroxy-7-quinolinyl)methyl)-1,10-diaza-18-crown-6 Ethers,” *J. Org. Chem.*, vol. 75, no. 18, pp. 6275–6278, Sep. 2010.
- [123] A. E. Palmer, Y. Qin, J. G. Park, and J. E. McCombs, “Design and application of genetically encoded biosensors,” *Trends Biotechnol.*, vol. 29, no. 3, pp. 144–152, Mar. 2011.
- [124] L. H. Lindenburg, J. L. Vinkenburg, J. Oortwijn, S. J. A. Aper, and M. Merckx, “MagFRET: The First Genetically Encoded Fluorescent Mg<sup>2+</sup> Sensor,” *PLoS ONE*, vol. 8, no. 12, p. e82009, Dec. 2013.

- [125] E. Malucelli, S. Iotti, A. Gianoncelli, M. Fratini, L. Merolle, A. Notargiacomo, C. Marraccini, A. Sargenti, C. Cappadone, G. Farruggia, I. Bukreeva, M. Lombardo, C. Trombini, J. A. Maier, and S. Lagomarsino, "Quantitative Chemical Imaging of the Intracellular Spatial Distribution of Fundamental Elements and Light Metals in Single Cells," *Anal. Chem.*, vol. 86, no. 10, pp. 5108–5115, May 2014.
- [126] C. Petibois, "Imaging methods for elemental, chemical, molecular, and morphological analyses of single cells," *Anal. Bioanal. Chem.*, vol. 397, no. 6, pp. 2051–2065, Jul. 2010.
- [127] R. Ortega, G. Devès, and A. Carmona, "Bio-metals imaging and speciation in cells using proton and synchrotron radiation X-ray micro-spectroscopy," *J. R. Soc. Interface*, p. rsif20090166, Jul. 2009.
- [128] S. Lagomarsino, S. Iotti, G. Farruggia, A. Cedola, V. Trapani, M. Fratini, I. Bukreeva, A. Notargiacomo, L. Mastrototaro, C. Marraccini, A. Sorrentino, I. McNulty, S. Vogt, D. Legnini, S. Kim, A. Gianoncelli, J. A. M. Maier, and F. I. Wolf, "Intracellular concentration map of magnesium in whole cells by combined use of X-ray fluorescence microscopy and atomic force microscopy," *Spectrochim. Acta Part B At. Spectrosc.*, vol. 66, no. 11–12, pp. 834–840, Nov. 2011.
- [129] M. W. Pfaffl, "A new mathematical model for relative quantification in real-time RT-PCR," *Nucleic Acids Res.*, vol. 29, no. 9, pp. e45–e45, May 2001.
- [130] D. Thomas, S. C. Tovey, T. J. Collins, M. D. Bootman, M. J. Berridge, and P. Lipp, "A comparison of fluorescent Ca<sup>2+</sup> indicator properties and their use in measuring elementary and global Ca<sup>2+</sup> signals," *Cell Calcium*, vol. 28, no. 4, pp. 213–223, Oct. 2000.
- [131] W. J. M. Scheenen, L. R. Makings, L. R. Gross, T. Pozzan, and R. Y. Tsien, "Photodegradation of indo-1 and its effect on apparent Ca<sup>2+</sup> concentrations," *Chem. Biol.*, vol. 3, no. 9, pp. 765–774, Sep. 1996.
- [132] P. J. Tadrous, "Methods for imaging the structure and function of living tissues and cells: 2. Fluorescence lifetime imaging," *J. Pathol.*, vol. 191, no. 3, pp. 229–234, Jul. 2000.
- [133] V. Trapani, F. Luongo, D. Arduini, and F. I. Wolf, "Magnesium modulates doxorubicin activity through drug lysosomal sequestration and trafficking," *Chem. Res. Toxicol.*, Feb. 2016.
- [134] G. Cavallari, E. Olivi, F. Bianchi, F. Neri, L. Foroni, S. Valente, G. La Manna, B. Nardo, S. Stefoni, and C. Ventura, "Mesenchymal Stem Cells and Islet Cotransplantation in Diabetic Rats: Improved Islet Graft Revascularization and Function by Human Adipose Tissue-Derived Stem Cells Preconditioned With Natural Molecules," *Cell Transplant.*, vol. 21, no. 12, pp. 2771–2781, Dec. 2012.

- [135] A. M. Singh, "Cell Cycle-Driven Heterogeneity: On the Road to Demystifying the Transitions between Poised and Restricted Pluripotent Cell States," *Stem Cells Int.*, vol. 2015, p. e219514, Apr. 2015.
- [136] F. Sato, Y. Matsukawa, K. Matsumoto, H. Nishino, and T. Sakai, "Apigenin Induces Morphological Differentiation and G2-M Arrest in Rat Neuronal Cells," *Biochem. Biophys. Res. Commun.*, vol. 204, no. 2, pp. 578–584, Oct. 1994.
- [137] R. Zarrilli, S. Pignata, A. Apicella, A. Di Popolo, A. Memoli, P. Ricchi, S. Salzano, and A. M. Acquaviva, "Cell cycle block at G1-S or G2-M phase correlates with differentiation of Caco-2 cells: Effect of constitutive insulin-like growth factor II expression," *Gastroenterology*, vol. 116, no. 6, pp. 1358–1366, Jun. 1999.
- [138] T. Kurita-Ochiai, T. Hashizume, H. Yonezawa, K. Ochiai, and M. Yamamoto, "Characterization of the effects of butyric acid on cell proliferation, cell cycle distribution and apoptosis," *FEMS Immunol. Med. Microbiol.*, vol. 47, no. 1, pp. 67–74, Jun. 2006.
- [139] C. Ventura, S. Cantoni, F. Bianchi, V. Lionetti, C. Cavallini, I. Scarlata, L. Foroni, M. Maioli, L. Bonsi, F. Alviano, V. Fossati, G. P. Bagnara, G. Pasquinelli, F. A. Recchia, and A. Perbellini, "Hyaluronan Mixed Esters of Butyric and Retinoic Acid Drive Cardiac and Endothelial Fate in Term Placenta Human Mesenchymal Stem Cells and Enhance Cardiac Repair in Infarcted Rat Hearts," *J. Biol. Chem.*, vol. 282, no. 19, pp. 14243–14252, May 2007.
- [140] R. J. Arceci, A. A. King, M. C. Simon, S. H. Orkin, and D. B. Wilson, "Mouse GATA-4: a retinoic acid-inducible GATA-binding transcription factor expressed in endodermally derived tissues and heart," *Mol. Cell. Biol.*, vol. 13, no. 4, pp. 2235–2246, Apr. 1993.
- [141] T. J. Lints, L. M. Parsons, L. Hartley, I. Lyons, and R. P. Harvey, "Nkx-2.5: a novel murine homeobox gene expressed in early heart progenitor cells and their myogenic descendants," *Development*, vol. 119, no. 2, pp. 419–431, Oct. 1993.
- [142] D. G. Duda, D. Fukumura, and R. K. Jain, "Role of eNOS in neovascularization: NO for endothelial progenitor cells," *Trends Mol. Med.*, vol. 10, no. 4, pp. 143–145, Apr. 2004.
- [143] H. He, V. J. Venema, X. Gu, R. C. Venema, M. B. Marrero, and R. B. Caldwell, "Vascular Endothelial Growth Factor Signals Endothelial Cell Production of Nitric Oxide and Prostacyclin through Flk-1/KDR Activation of c-Src," *J. Biol. Chem.*, vol. 274, no. 35, pp. 25130–25135, Aug. 1999.
- [144] S. J. Morrison, "Neuronal differentiation: Proneural genes inhibit gliogenesis," *Curr. Biol.*, vol. 11, no. 9, pp. R349–R351, May 2001.
- [145] K. Mitsui, Y. Tokuzawa, H. Itoh, K. Segawa, M. Murakami, K. Takahashi, M. Maruyama, M. Maeda, and S. Yamanaka, "The Homeoprotein Nanog Is Required

for Maintenance of Pluripotency in Mouse Epiblast and ES Cells," *Cell*, vol. 113, no. 5, pp. 631–642, May 2003.

- [146] A. Sargenti, G. Farruggia, E. Malucelli, C. Cappadone, L. Merolle, C. Marraccini, G. Andreani, L. Prodi, N. Zaccheroni, M. Sgarzi, C. Trombini, M. Lombardo, and S. Iotti, "A novel fluorescent chemosensor allows the assessment of intracellular total magnesium in small samples," *Analyst*, vol. 139, no. 5, pp. 1201–1207, 2014.
- [147] S. Castiglioni, A. Cazzaniga, V. Trapani, C. Cappadone, G. Farruggia, L. Merolle, F. I. Wolf, S. Iotti, and J. A. M. Maier, "Magnesium homeostasis in colon carcinoma LoVo cells sensitive or resistant to doxorubicin," *Sci. Rep.*, vol. 5, 2015.